WALL TEMPERATURE EFFECTS ON TWO- AND THREE-DIMENSIONAL TRANSONIC TURBULENT BOUNDARY LAYERS

J. C. Adams, Jr. and A. W. Mayne, Jr.

ARO, Inc.

October 1973

VON KÁRMÁN GAS DYNAMICS FACILITY
ARNOLD ENGINEERING DEVELOPMENT CENTER
AIR FORCE SYSTEMS COMMAND
ARNOLD AIR FORCE STATION, TENNESSEE

NOTICES

When U. S. Government drawings specifications, or other data are used for any purpose other than a definitely related Government procurement operation, the Government thereby incurs no responsibility nor any obligation whatsoever, and the fact that the Government may have formulated, furnished, or in any way supplied the said drawings, specifications, or other data, is not to be regarded by implication or otherwise, or in any manner licensing the holder or any other person or corporation, or conveying any rights or permission to manufacture, use, or sell any patented invention that may in any way be related thereto.

Qualified users may obtain copies of this report from the Defense Documentation Center.

References to named commercial products in this report are not to be considered in any sense as an endorsement of the product by the United States Air Force or the Government.

WALL TEMPERATURE EFFECTS ON TWO- AND THREE-DIMENSIONAL TRANSONIC TURBULENT BOUNDARY LAYERS

J. C. Adams, Jr. and A. W. Mayne, Jr.
ARO, Inc.

FOREWORD

The work reported herein was conducted by the Arnold Engineering Development Center (AEDC), Air Force Systems Command (AFSC), under Program Element 65802F.

The results of research presented were obtained by ARO, Inc. (a subsidiary of Sverdrup & Parcel and Associates, Inc.), contract operator of AEDC, AFSC, Arnold Air Force Station, Tennessee. The research was conducted from December 1972 until July 1973 under ARO Projects Nos. VD205 and VF405, and the manuscript was submitted for publication on July 12, 1973.

This technical report has been reviewed and is approved.

ROSS G. ROEPKE
Requirements Planning Division
Directorate of Technology

ROBERT O. DIETZ
Director of Technology

ABSTRACT

Wall temperature effects on the two- and three-dimensional high Reynolds number turbulent boundary layer are examined for representative AEDC High Reynolds Number Tunnel (HIRT) conditions relative to flight; also considered are hot-wall conditions relative to Space Shuttle subsonic and transonic flight during earth entry. Results obtained and presented herein show significant influences of wall-to-stagnation temperature ratio on the location of boundary-layer separation and the friction drag coefficient. The present study also indicates that the model wall temperature will be rapidly changing during a typical HIRT testing period of from 2 to 10 sec if the model is initially at ambient room temperature; such a condition may be undesirable for HIRT testing in the sweeping pitch mode since unsteady aerodynamic phenomena (e.g., airfoil dynamic stall) can be influenced by rapidly changing turbulent boundary-layer wall temperature levels. Ground testing of Space Shuttle configurations under continuous transonic flow conditions with an adiabatic wall may not be totally applicable to actual Shuttle entry, where the wing surface temperature can reach soak values on the order of twice the free-stream stagnation temperature because of the hypersonic high heating phase of the reentry trajectory. Simulation of this hot-wall/cold free-stream environment using electrically heated models appears necessary for continuous subsonic and transonic wind tunnel testing of Shuttle configurations, especially for aerodynamic drag and stall characteristics determination.

CONTENTS

APPENDIX
ILLUSTRATIONS

Figure

NOMENCLATURE

A_*	Van Driest damping constant, 26.0
C_{f_e}	Local skin-friction coefficient referenced to inviscid edge conditions, $2\tau_w/\rho_e U_e^2$
C_{f_∞}	Local skin-friction coefficient referenced to free-stream conditions, $2\tau_w/\rho_\infty V_\infty^2$
$C_{L_{max}}$	Maximum value for aerodynamic lift coefficient
C_p	Local surface pressure coefficient referenced to free-stream conditions, $2(p_e-p_\infty)/\rho_\infty V_\infty^2$
c	Airfoil chord length
c_p	Constant pressure specific heat
H	Boundary-layer shape factor, δ^*/θ
$\bar{h}$	Mean static enthalpy
k	Thermal conductivity

k_*	Inner law mixing-length constant, 0.435
ℓ_*	Mixing length
M_e	Local surface inviscid Mach number
M_∞	Free-stream Mach number
Pr	Laminar Prandtl number, 0.71
Pr_t	Turbulent Prandtl number, 0.90
p_e	Local surface inviscid static pressure
$p_o)_\infty$	Free-stream stagnation pressure
p_∞	Free-stream static pressure
$\dot{q}$ or $\dot{q}_w$	Local surface heat flux
$Re_{\infty, c}$	Free-stream Reynolds number based on airfoil chord length, $(\rho_\infty V_\infty c)/\mu_\infty$
T_{aw}	Local adiabatic wall temperature
$T_o)_\infty$ or $T_{o,\infty}$	Free-stream stagnation temperature
T_w	Local wall temperature
T_∞	Free-stream static temperature
U_e	x-direction velocity component at outer edge of boundary layer
U_∞	x-direction velocity component in free-stream
$\overline{u}$	x-direction velocity component in boundary layer
V_∞	Free-stream velocity
$\overline{v}$	y-direction velocity component in boundary layer
W_e	z-direction velocity component at outer edge of boundary layer
W_∞	z-direction velocity component in free stream
$\overline{w}$	z-direction velocity component in boundary layer
X	Distance in chordwise direction (see Fig. 3)
x	Streamwise surface coordinate (see Figs. 1, 2, and 3)
x_{max}	Maximum value of the x-coordinate

y	Coordinate normal to body surface (see Figs. 1, 2, and 3)
y_ℓ	Characteristic thickness of boundary layer given by Eq. (11)
z	Crossflow surface coordinate (see Figs. 2 and 3)
α	Airfoil angle of attack
α_{stall}	Airfoil stall angle of attack
δ^*	Displacement thickness, $\delta^* = \int_0^\infty \left(1 - \frac{\bar{\rho}\,\bar{u}}{\rho_e U_e}\right) dy$
δ_x^*	Displacement thickness in x-direction, $\delta_x^* = \int_0^\infty \left(1 - \frac{\bar{\rho}\,\bar{u}}{\rho_e U_e}\right) dy$
δ_z^*	Displacement thickness in z-direction, $\delta_z^* = \int_0^\infty \left(1 - \frac{\bar{\rho}\,\bar{w}}{\rho_e W_e}\right) dy$
ϵ	Eddy viscosity
ϵ_i	Eddy viscosity in inner region
ϵ_o	Eddy viscosity in outer region
θ	Momentum thickness, $\theta = \int_0^\infty \frac{\bar{\rho}\,\bar{u}}{\rho_e U_e}\left(1 - \frac{\bar{u}}{U_e}\right) dy$
$\theta_{m,x}$	Momentum thickness in x-direction, $\theta_{m,x} = \int_0^\infty \frac{\bar{\rho}\,\bar{u}}{\rho_e U_e}\left(1 - \frac{\bar{u}}{U_e}\right) dy$
$\theta_{m,z}$	Momentum thickness in z-direction, $\theta_{m,z} = \int_0^\infty \frac{\bar{\rho}\,\bar{w}}{\rho_e W_e}\left(1 - \frac{\bar{w}}{W_e}\right) dy$
κ	Eddy thermal conductivity
Λ	Airfoil sweep angle
λ	Outer law mixing-length constant, 0.09
μ	Laminar (molecular) viscosity
μ_∞	Free-stream viscosity
$\bar{\rho}$	Mean mass density
ρ_e	Mass density at outer edge of the boundary layer
ρ_∞	Free-stream mass density

τ_{turb}	Turbulent shear stress
τ_w	Wall shear stress
ω	Local streamline angle (see Fig. 3)
ω_e	Local streamline angle at outer edge of boundary layer
ω_s	Local limiting streamline angle at body surface

SUBSCRIPTS

x	x-coordinate direction
z	z-coordinate direction
∞	Free-stream conditions

SUPERSCRIPTS

$( )'$	Fluctuating component
$(\bar{})$	Average with respect to time

SECTION I
INTRODUCTION

In a recent (unpublished) paper (Ref. 1), Green, Weeks, and Pugh investigated the influence of the ratio of the wall temperature to the free-stream stagnation temperature on the turbulent boundary-layer flow over the upper surface of an airfoil in a Mach 0.664 free-stream flow. They concluded that, at conditions similar to those encountered in a Ludwieg-tube-driven high Reynolds number transonic test facility, the effects of the increase in Reynolds number obtained by the stagnation temperature reduction caused by the unsteady expansion wave are negated by the influences of a higher than adiabatic wall-to-stagnation temperature ratio resulting when an uncooled model is used.

The method used to obtain the results given in Ref. 1 was basically Head's integral entrainment method (Ref. 2). Although this is reputed to be a relatively good method for calculating compressible turbulent boundary-layer flows, it was decided to check the results and conclusions of Ref. 1 by performing similar calculations using the finite-difference methods which have been developed in the AEDC von Kármán Gas Dynamics Facility (VKF) for treating such flows. The reason for this test of the Ref. 1 results is their ramifications for the High Reynolds Number Tunnel (HIRT) Ludwieg-tube-driven facility currently under development in VKF (Ref. 3). Particular parameters of interest which are influenced by the wall-to-stagnation temperature ratio are the coefficient of skin friction, the location of boundary-layer separation, and the friction drag coefficient. In addition to the tests on the results of Ref. 1, three other series of calculations were performed to investigate the effects of wall-to-stagnation temperature ratio on turbulent boundary-layer flow; these results are also presented in this report.

Two finite-difference methods for numerical calculation of compressible turbulent boundary layers were used in the present investigation. Both methods utilize the eddy transport coefficient hypothesis for treating the turbulent momentum and energy fluxes, but the two methods are completely independent. The first method is a modified version of the scheme originally developed by Patankar and Spalding (Ref. 4). This method treats the boundary-layer equations in a von Mises variables form, and its use in VKF has been described in Refs. 5 and 6. The second method used in this investigation was that developed by Adams (Refs. 7 and 8) for treating the three-dimensional boundary-layer flow over an infinite yawed wing.

In addition to its relevance to testing in the HIRT facility, the influence of unmatched wall-to-stagnation temperature ratio on turbulent boundary-layer flow may be significant in wind tunnel tests simulating the transonic phase of the Space Shuttle Orbiter reentry, and results of investigations into this problem are included in the present report. There is an interesting contrast between the wall temperature ratio simulation problem for aircraft testing in HIRT and Space Shuttle Orbiter reentry testing in a continuous wind tunnel. In HIRT the wall-to-stagnation temperature ratio of an uncooled model will be higher than the adiabatic wall value, which is essentially the flight condition to be simulated. In continuous tunnel transonic flow testing of a Space Shuttle Orbiter, however, the model surface will typically be at an adiabatic wall temperature condition, rather than at some higher temperature condition which may be imposed on the flight vehicle by aerodynamic heating during the supersonic and hypersonic portions of the reentry flight.

SECTION II
METHODS OF CALCULATION

Two different methods of treating the compressible turbulent boundary-layer equations have been used in this investigation. Both approaches utilize finite-difference methods of solving the boundary-layer equations in which the turbulent momentum and energy flux terms resulting from Reynolds averaging are treated by the eddy transport coefficient hypothesis. All calculations are for thermally and calorically perfect air and use the Sutherland law for the laminar viscosity.

2.1 PATANKAR-SPALDING METHOD

The first method used in the present study is based on the theory and numerical scheme first developed by Patankar and Spalding (Ref. 4), although the treatment used in this investigation is a highly modified form of their work and may be considered an extension of the work reported by Mayne and Dyer in Ref. 5.

In this approach, the boundary-layer equations for two-dimensional and axisymmetric flows are transformed into a normalized von Mises coordinate system and are numerically solved using a marching, implicit finite-difference procedure. The exact form of the boundary-

layer equations used may be found in Refs. 5 and 6. The turbulent transport formulations used were the two-dimensional counterparts of those given in Sections 2.3 and 2.4. A sketch indicating the airfoil situation under present consideration and showing some of the primary variables is given in Fig. 1, Appendix.

In applying this method, the boundary-layer profiles were approximated at an initial location close to the stagnation line, and the solution method proceeded downstream from that point. It has been determined that the initial profiles used have no significant influence on the results obtained downstream, provided that the initial profiles are not entirely unreasonable. In some of the calculations made in this investigation, the initial state of the boundary layer was specified to be laminar, with transition occurring shortly past the initial location, whereas in other calculations the initial state was specified to be turbulent. This assumption had no significant influence on the results obtained over the aft part of the surface.

Conditions along the outer edge of the boundary layer were determined by specifying the conditions in the uniform free stream ahead of the airfoil, together with the variation of the static pressure in the inviscid flow over the surface. The variation of the inviscid flow variables along the outer edge of the boundary layer was computed using this information and isentropic flow relationships.

In applying the Patankar-Spalding method, the surface boundary condition on the energy equation was specified by fixing the surface temperature at a constant value or by requiring the surface to be adiabatic.

The results obtained from numerical solution of the boundary-layer equations are the values of velocity, density, etc., at a set of points on normals to the body surface, at a series of locations along the surface. These data are integrated, differentiated, interpolated, etc., to provide values of the surface heat-transfer rate and shearing stress, the displacement thickness, the momentum thickness, and other boundary-layer parameters of interest.

All of the Patankar-Spalding boundary-layer calculations in the present report were performed using the VKF CDC 1604-B digital computer with the program written in FORTRAN 63. Typical execution times for a complete boundary-layer calculation averaged from 50 to 70 minutes using approximately 800 x-direction stations along the airfoil; in all cases, 200 points were used in the y-direction with a variable y-direction grid employed to concentrate grid points in the near-wall region.

Basic validity, applicability, and accuracy of the Patankar-Spalding method applied to turbulent boundary-layer flows under subsonic, transonic, supersonic, and hypersonic flow conditions may be found in the following references:

1. Patankar and Spalding (Ref. 4),
2. Mayne and Dyer (Ref. 5),
3. Launder and Spalding (Ref. 9, pp. 30-33), and
4. Sivasegaram and Whitelaw (Ref. 10).

2.2 INFINITE YAWED WING TREATMENT

The second method used in the present study is based on the infinite yawed body theory and numerical scheme developed by Adams (Refs. 7 and 8). In this approach, the three-dimensional compressible turbulent boundary-layer equations for an infinite yawed body are transformed using the Illingworth-Levy transformation and are numerically solved using a marching, implicit finite-difference procedure. (See Appendix III of Refs. 7 and 8 for complete details of the numerical procedure.) The exact form of the three-dimensional boundary-layer equations may be found in Sections II of Refs. 7 and 8; the three-dimensional turbulent transport formulations are given in Sections 2.3 and 2.4 of the present report. The infinite yawed body geometry and nomenclature adopted for the current study are given in Fig. 2. Note that the airfoil is assumed to be infinite in extent; this assumption results in the condition that all partial derivative terms in $\partial/\partial z$ are set to zero in the governing equations of motion.

Details of the infinite yawed body geometry and nomenclature as applied to a swept airfoil are given in Fig. 3. With reference to Fig. 3a, note that the definition of three-dimensional boundary-layer separation on an infinite yawed wing is taken to be the chordwise line along which the x-direction component of the local skin friction vanishes (see pages 107 through 109 in the recent book by Nash and Patel, Ref. 11, for a general discussion of three-dimensional boundary-layer separation). Further note from Fig. 3a that the chordwise flow separation line on an infinite yawed wing can be physically identified by the location where the limiting surface streamline turns back parallel with the leading edge so that the surface flow angle, ω_s, becomes zero.

In applying the infinite yawed wing boundary-layer analysis, the boundary layer was taken to be laminar along the stagnation or attachment line (see Fig. 2 for clarification); the method of numerical solution

for the stagnation or attachment line flow is discussed in Appendix III of both Refs. 7 and 8. Boundary-layer transition on the swept airfoil was assumed to be solely controlled by crossflow instability (Refs. 12 and 13) with a step-jump transition from laminar to turbulent flow at the x-location on the airfoil where the so-called crossflow Reynolds number attained a value of 200. (See Refs. 7, 8, 12, and 13 for definition and discussion of the crossflow Reynolds number in terms of three-dimensional laminar boundary-layer parameters.)

Conditions along the outer edge of the yawed wing boundary layer were determined by specifying the conditions in the uniform free stream ahead of the airfoil, together with the variation of the static pressure in the inviscid flow over the surface based on classical inviscid sweep theory. The variation of the inviscid flow variables along the outer edge of the boundary layer was computed using this information and isentropic flow relationships.

For the infinite yawed wing analysis, the surface boundary condition on the energy equation was specified by fixing the surface temperature at a constant value or requiring the surface to be adiabatic, just as in the Patankar-Spalding method. The results from numerical solution of the infinite yawed body boundary-layer equations have been applied in exactly the same manner as the Patankar-Spalding results discussed in Section 2.1.

All of the infinite yawed airfoil boundary-layer calculations in the present report have been performed using the VKF CDC 1604-B digital computer with the program written in FORTRAN 63. Typical execution times for a complete yawed wing boundary-layer calculation averaged from 60 to 90 minutes using a variable x-direction step size in order to accurately define the three-dimensional separation line; in all cases, 96 points were used in the y-direction with a variable y-direction grid employed to concentrate grid points in the near-wall region.

Little work has been done to date in the area of calculation techniques for three-dimensional compressible turbulent boundary layers on infinite yawed wings. A recent report by Adams (Ref. 8) established the accuracy of the present yawed wing approach under subsonic conditions. Included in this report were comparisons of the present technique relative to the kinetic-energy-of-turbulence analysis by Nash and Tseng (Ref. 14) on a 35-deg infinite swept wing with a symmetrical, 12-percent-thick NACA 65_1A012 airfoil section in the chordwise direction; the free-stream Reynolds number based on the streamwise chord, $c/\cos\Lambda$, has

a value of 75 million, which corresponds to full-scale conditions for a large transport aircraft. As shown in the recent report by Hicks and Nash (Ref. 15), infinite yawed wing calculations are in excellent agreement with fully three-dimensional calculations for turbulent boundary layers on swept wings of high aspect ratio.

2.3 TURBULENT TRANSPORT MODEL

Before the governing boundary-layer equations can be solved, expressions must be supplied for the Reynolds stress or turbulent shear terms in the momentum equations and for the turbulent flux of total energy in the energy equation. The approach used in the present analyses is to model these terms as functions of the mean-flow variables. An outline of this modeling procedure is given below with respect to the three-dimensional turbulent boundary layer; for two-dimensional turbulent boundary-layer flows, the z-direction velocity component ($\overline{w}$) is identically zero, which is used to reduce the three-dimensional expressions to their two-dimensional counterparts.

The concept that the Reynolds stress in turbulent flow is proportional to a momentum exchange coefficient times the mean-flow velocity gradient normal to the surface is well known and commonly used in turbulent boundary-layer analyses. This concept is based on an assumed analogy between the so-called eddy viscosity and the molecular viscosity. The total shear components in the x- and z-directions are written as

$$\tau_x = \mu \frac{\partial \overline{u}}{\partial y} - \overline{\rho}\,\overline{u'v'} = \mu \frac{\partial \overline{u}}{\partial y} + \epsilon_x \frac{\partial \overline{u}}{\partial y} \tag{1}$$

$$\tau_z = \mu \frac{\partial \overline{w}}{\partial y} - \overline{\rho}\,\overline{v'w'} = \mu \frac{\partial \overline{w}}{\partial y} + \epsilon_z \frac{\partial \overline{w}}{\partial y} \tag{2}$$

where the eddy viscosities ϵ_x and ϵ_z in the x- and z-directions, respectively, might in general be different. Applying the Prandtl mixing-length hypothesis in conjunction with the assumption that the eddy viscosity is a scalar function independent of coordinate direction (which means physically that the turbulent shear stress acts in the mean rate of strain direction) results in an eddy viscosity relationship of the form

$$\epsilon = \epsilon_x = \epsilon_z = \overline{\rho} \ell_*^2 \frac{\partial \overline{G}}{\partial y} \tag{3}$$

where $\overline{G}$ is a scalar velocity function defined by

$$\frac{\partial \overline{G}}{\partial y} = \left[\left(\frac{\partial \overline{u}}{\partial y}\right)^2 + \left(\frac{\partial \overline{w}}{\partial y}\right)^2\right]^{1/2} \tag{4}$$

The quantity ℓ_* is termed the mixing length and is some characteristic length related to the size or scales of eddies responsible for the flux of momentum in the y-direction. Under the above model the turbulent shear stress in a three-dimensional turbulent boundary layer may be written in the form

$$\tau_{turb} = \overline{\rho}\ell_*^2\left[\left(\frac{\partial \overline{u}}{\partial y}\right)^2 + \left(\frac{\partial \overline{w}}{\partial y}\right)^2\right] \tag{5}$$

The complete derivation of Eqs. (3), (4), and (5) is given in Refs. 16, 17, and 18.

The expression for the total heat flux in a turbulent boundary layer may be written in terms of the static enthalpy as

$$\dot{q} = \frac{k}{c_p}\frac{\partial \overline{h}}{\partial y} - \overline{\rho}\,\overline{v'h'} = \frac{k}{c_p}\frac{\partial \overline{h}}{\partial y} + \frac{\kappa}{c_p}\frac{\partial \overline{h}}{\partial y} \tag{6}$$

where k is the laminar (molecular) thermal conductivity and κ is the so-called eddy thermal conductivity. Using the definition of the laminar (molecular) Prandtl number

$$Pr = \frac{c_p\mu}{k} \tag{7}$$

and defining, by analogy, a turbulent Prandtl number (based on the use of static enthalpy) as

$$Pr_t = \frac{c_p\epsilon}{\kappa} \tag{8}$$

with ϵ the eddy viscosity discussed previously, the total heat flux expression (6) may be written in the form

$$\dot{q} = \mu\left[\frac{1}{Pr} + \frac{\epsilon}{\mu}\frac{1}{Pr_t}\right]\frac{\partial \overline{h}}{\partial y} \tag{9}$$

2.4 MIXING-LENGTH MODEL

The turbulent shear stress in a three-dimensional turbulent boundary layer as governed by Eq. (5) is treated herein by the use of a two-layer inner-outer model using Prandtl's mixing-length hypothesis and a modification of van Driest's analysis for the near-wall region. This results in a continuous distribution of the shear stress from the laminar value at the wall, through the fully turbulent region, reaching zero at the outer edge of the boundary layer. The energy transport in a turbulent boundary layer is treated in this work through the incorporation of the eddy conductivity, κ, into the turbulent Prandtl number, Pr_t.

In the manner of Escudier (Ref. 19), Patankar and Spalding (Ref. 4) recommend the following variation of the mixing length, ℓ_*, across the turbulent two-dimensional boundary layer which is adopted for the present three-dimensional case by noting that the scalar properties of a turbulence field are unlikely to be affected by moderate three-dimensionality because turbulence is inherently three-dimensional in nature for even so-called two-dimensional flows:

$$\left.\begin{aligned} \ell_* &= k_* y, \text{ for } 0 < y \leq \lambda y_\ell / k_* \\ \ell_* &= \lambda y_\ell, \text{ for } \lambda y_\ell / k_* < y \end{aligned}\right\} \tag{10}$$

where the values for the various numerical constants are taken to be $k_* = 0.435$ and $\lambda = 0.09$. The value of y at the point where the velocity in the boundary layer is equal to 0.99 of the velocity at the boundary-layer outer edge is used to define the distance y_ℓ; i.e.,

$$y_\ell = \left\{ \text{y-value where } \frac{\left[(\bar{u})^2 + (\bar{w})^2\right]^{1/2}}{\left[(U_e)^2 + (W_e)^2\right]^{1/2}} = 0.99 \right\} \tag{11}$$

By analogy with Stokes' solution for an infinite flat plate undergoing simple harmonic motion parallel to itself in an infinite fluid, van Driest (Ref. 20) concluded that in the vicinity of a wall the total shear stress in a turbulent two-dimensional fluid should be of the form

$$\tau = \mu \frac{\partial \bar{u}}{\partial y} + \bar{\rho} k_*^2 y^2 \left[1 - \exp\left(\frac{-y\sqrt{\tau_w \bar{\rho}}}{\mu A_*}\right)\right]^2 \left(\frac{\partial \bar{u}}{\partial y}\right)^2 \tag{12}$$

which results in an exponential damping of the turbulent part of the shear stress as the wall is approached and yields exactly the laminar shear stress form, $\tau = \mu(\partial\bar{u}/\partial y)$, at the wall. Although Eq. (12) was originally developed for incompressible flow, it can be applied to compressible flow by application of the suggestion by Patankar and Spalding (Ref. 4) that the local value of shear stress be used instead of the wall value as originally recommended by van Driest (Ref. 20). Hence, by analogy between Eq. (12) and Eqs. (4) and (5), the relationship for the three-dimensional near-wall shear stress as used in the present analysis is

$$\tau = \mu \frac{\partial \bar{G}}{\partial y} + \bar{\rho} k_*^2 y^2 \left[1 - \exp\left(\frac{-y\sqrt{\tau\bar{\rho}}}{\mu A_*}\right)\right]^2 \left(\frac{\partial \bar{G}}{\partial y}\right)^2 \tag{13}$$

where the constant A_* is taken to be 26.0, following the original van Driest proposal (Ref. 20). Note that the damping term in Eq. (13) reflects the application of the local total shear stress as opposed to the wall shear stress of Eq. (12), as discussed previously.

Based on Eqs. (3), (4), (10), and (13), the eddy viscosity expression for the inner region is

$$\epsilon_i = \bar{\rho} k_*^2 y^2 \left[1 - \exp\left(\frac{-y\sqrt{\tau\bar{\rho}}}{\mu A_*}\right)\right]^2 \frac{\partial \bar{G}}{\partial y} \tag{14}$$

and for the outer region is

$$\epsilon_o = \bar{\rho} \lambda^2 y_\ell^2 \frac{\partial \bar{G}}{\partial y} \tag{15}$$

with the constants k_*, A_*, λ, and y_ℓ defined previously. The constraint used to define the end of the inner region and the beginning of the outer region is the continuity of the eddy viscosity. From the wall outward, the expression for the inner eddy viscosity applies until $\epsilon_i = \epsilon_o$, from which point the outer eddy viscosity is used. A schematic of this variation in terms of the mixing lengths follows.

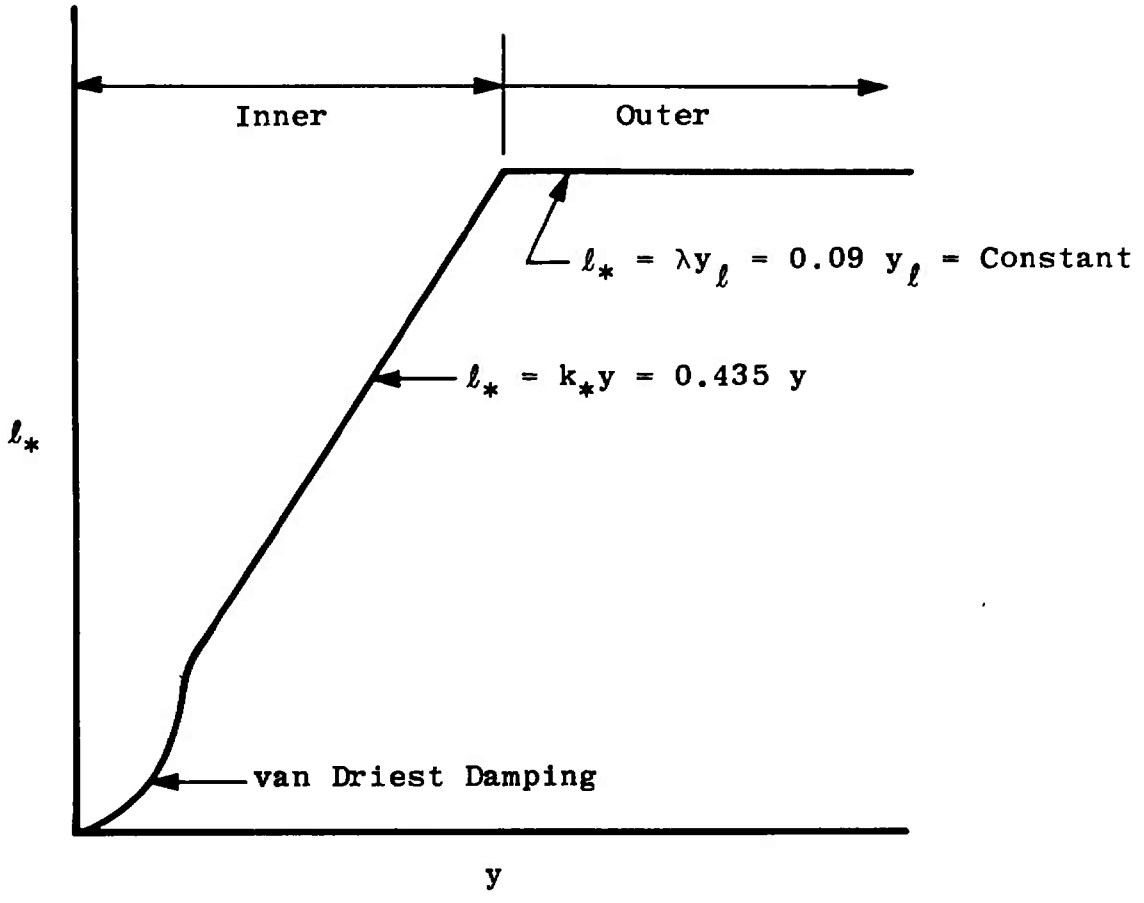

The turbulent Prandtl number (based on the static enthalpy definition of the turbulent heat flux) as given by Eq. (8) is physically a measure of the ratio of the turbulent transport of momentum to the turbulent transport of heat. For the present work, the turbulent Prandtl number defined by Eq. (8) is taken to remain constant at the value 0.90 across the entire boundary layer as recommended by Patankar and Spalding (Ref. 4) for two-dimensional turbulent boundary layers.

SECTION III
RESULTS AND DISCUSSION

In this section are presented the results of four sets of calculations which have been performed to investigate the influence of a greater-

than-adiabatic wall-to-stagnation temperature ratio on the turbulent boundary-layer flow over a body in transonic flow. The first set of calculations is for a situation essentially like that of Ref. 1, namely, an airfoil in a Mach 0.664 flow. For this case, wall-to-stagnation temperature ratio influences are compared with changes induced by varying the free-stream Reynolds number. The second case considered is that of an unyawed wing in a Mach 0.815 flow at conditions typical of the proposed HIRT facility. The third case is that of a yawed wing in a Mach 0.815 flow, and the final case considers wall-to-stagnation temperature ratio effects on wind tunnel simulations of turbulent boundary-layer flow over a hot surface such as might be encountered on a Space Shuttle Orbiter wing during earth entry.

All of the results obtained in this investigation indicate that wind tunnel tests of airfoils in transonic flows should attempt to match the flight wall-to-stagnation temperature ratio in order to properly simulate actual flight conditions.

3.1 AIRFOIL IN MACH 0.664 FLOW

In Ref. 1, the turbulent boundary-layer flow over an airfoil in a Mach 0.664 free stream is treated theoretically using an integral entrainment method. In the present investigation, a case which is essentially the same as that of Ref. 1 has been considered using the method described in Section 2.1.

The conditions used for this case were as follows:

$$M_\infty = 0.664$$

$$T_W = 310°K = 558°R$$

$$(T_W/T_O)_\infty = 0.99,\ 1.04,\ 1.07,\ \text{and } 1.10$$

$$Re_{\infty, c} = 40 \times 10^6 \text{ and } 35 \times 10^6 \ [(T_W/T_O)_\infty = 0.99 \text{ only}]$$

$$c = 1.5 \text{ ft}$$

The basic value of $Re_{\infty, c}$ was 40×10^6, with each value of $(T_W/T_O)_\infty$ being considered at this Reynolds number. The lower Reynolds number condition, $Re_{\infty, c} = 35 \times 10^6$, was considered in order to compare Reynolds number influences with $(T_W/T_O)_\infty$ variation influences. The

$(T_w/T_o)_\infty = 0.99$ condition was used as a datum level of wall-to-stagnation temperature level; this value is essentially an adiabatic-wall temperature condition.

Figure 4 shows the surface pressure distribution used for this case. The coefficient of pressure is shown as a function of the dimensional and the nondimensional distance along the surface from the stagnation line. These data are an idealized version of those used in Ref. 1, which were said to be derived from the surface pressure distribution for an RAE Section 2815 airfoil. For this case, values of C_p less than approximately -0.96 indicate supersonic flow at the outer edge of the boundary layer. The data shown in Fig. 4 represent a highly accelerated flow over a short forward portion of the surface, a length of moderately accelerating flow, and continuously decelerating flow over the aft 70 percent of the surface.

The adverse pressure gradient is such that boundary-layer separation is reached near the trailing edge of the wing for all of the cases considered in this investigation, as shown in Fig. 5 by the distribution of the local coefficient of skin friction over the trailing-edge region. For $Re_{\infty, c} = 40 \times 10^6$ and $(T_w/T_o)_\infty = 1.10$, which is approximately the value of the wall temperature ratio for an uncooled model at this condition in the HIRT facility, the separation point is moved forward about one percent of the chord from its location with $(T_w/T_o)_\infty = 0.99$. This compares with a shift of only one-half of one percent in the separation location between the $Re_{\infty, c} = 40 \times 10^6$ and $Re_\infty = 35 \times 10^6$ cases, both cases having $(T_w/T_o)_\infty = 0.99$.

Considering the shape factor, H, as an indicator of the tendency of a boundary layer to separate, Fig. 6 shows that the results for the $Re_{\infty, c} = 40 \times 10^6$, $(T_w/T_o)_\infty = 1.10$ case are farther removed from the $Re_{\infty, c} = 40 \times 10^6$, $(T_w/T_o)_\infty = 0.99$ case results than the results for the $Re_{\infty, c} = 35 \times 10^6$, $(T_w/T_o)_\infty = 0.99$ case.

Figures 7, 8, 9, and 10 show the influence of increasing $(T_w/T_o)_\infty$ at constant $Re_{\infty, c}$ as opposed to decreasing $Re_{\infty, c}$ at constant $(T_w/T_o)_\infty$ on computed displacement thickness, momentum thickness, shape factor, and skin-friction coefficient. These figures each show the distribution of the ratio of the parameter under consideration at given values of $Re_{\infty, c}$ and $(T_w/T_o)_\infty$ to its value at $Re_{\infty, c} = 40 \times 10^6$ and $(T_w/T_o)_\infty = 0.99$. If there were no influence of variations in the Reynolds number or wall temperature ratio, the distributions would all be identically unity. For all of the parameters mentioned, except possibly the momentum thickness, the data for $Re_{\infty, c} = 40 \times 10^6$, $(T_w/T_o)_\infty = 1.10$ are farther from unity than the data for $Re_{\infty, c} = 35 \times 10^6$, $(T_w/T_o)_\infty = 0.99$.

In summary, the above results show that for the parameters considered the influence of an increase (or mismatch) of about 11 percent in $(T_w/T_o)_\infty$ is larger than the influence of a decrease in $Re_{\infty,c}$ of almost 13 percent.

3.2 TWO-DIMENSIONAL AIRFOIL IN MACH 0.815 HIRT FLOW

A series of calculations was performed for another two-dimensional airfoil case. The purpose of these calculations was to examine a situation more closely approximating the expected flow in HIRT and to compare the Patankar-Spalding method with the infinite yawed wing method of treating the turbulent boundary layer.

The case considered does not represent any specific airfoil, although the pressure distribution which is shown in Fig. 11 is similar to the chordwise pressure distribution used for the infinite yawed wing calculations presented in Section 3.3. The origins of this pressure distribution will be discussed there. Although this case does not yield computed boundary-layer separation in the two-dimensional case, it does lead to some significant results concerning the influences of $(T_w/T_o)_\infty$ on computed turbulent boundary-layer data.

For this set of calculations, the Reynolds number and other free-stream conditions were fixed, and only the influence of the wall temperature on computed turbulent boundary-layer data was considered. Specifically, the results of computations with $(T_w/T_o)_\infty = 1.103$ were compared with results for an adiabatic-wall situation. The free-stream conditions used were

$$M_\infty = 0.815$$

$$Re_{\infty,c} = 1.05 \times 10^8$$

$$(T_o)_\infty = 489°R,\ T_\infty = 432°R,\ T_w = 540°R$$

$$(p_o)_\infty = 325 \text{ psi},\ p_\infty = 210 \text{ psi}$$

$$c = 1.0 \text{ ft}$$

which are representative of the VKF HIRT facility. This free-stream Mach number/chord Reynolds number combination is also typical of full-scale flight conditions for a large transonic transport aircraft.

Figure 12 shows the distribution of C_{f_∞} along the wing for the two wall temperature conditions considered, with results being presented from both the Patankar-Spalding method and the infinite yawed wing method (at zero yaw). The results from the two methods agree quite well here, as they do in the succeeding four figures for other parameters. This demonstrates the consistency of the two methods and should serve to increase the confidence one has in the results obtained since each method has previously yielded results which show good agreement with a wide variety of experimental data for turbulent boundary-layer flows. The primary conclusion to be drawn from Fig. 12 is that the integrated skin-friction drag over the wing for the $(T_w/T_o)_\infty = 1.103$ case is approximately 4 percent less than that for the adiabatic wall temperature case. This is another factor pointing to the necessity for proper wall temperature ratio simulation in HIRT.

Figure 13 shows the distribution obtained for the ratio of the adiabatic-wall temperature to the free-stream total temperature. This ratio ranges from 0.975 to 0.995 with a mean of about 0.985, which is close to the 0.99 value used for the datum in Section 3.1.

Figure 14 shows the distribution of the shape factor, H, which was obtained for the two wall temperature conditions. Although the level for the $(T_w/T_o)_\infty = 1.103$ case is 10 to 15 percent higher than that for the adiabatic wall case over the entire airfoil, the flow does not approach sufficiently close to separation to allow any conclusion to be drawn concerning the relative positions of boundary-layer separation for the two cases.

Consideration of the displacement thickness distribution data in Fig. 15, together with the shape factor data in Fig. 14, yields the conclusion that the difference in the displacement thickness distributions for the two cases is the primary reason for the difference in the two shape factor distributions (i.e., H varies with δ^*, with θ approximately the same for the two conditions).

An interesting and not insignificant additional result obtained in this phase of the investigation was data concerning the surface heating rates computed for the $(T_w/T_o)_\infty = 1.103$ condition, which closely simulates a potential condition in the HIRT facility. Figure 16 shows the surface heat-transfer rate obtained for this case. The computed heat-transfer rate is over 25 Btu/ft^2-sec near the leading edge and falls to approximately 10 Btu/ft^2-sec at the trailing edge. These heating rates

represent heat transfer from the wall into the boundary layer, thus tending to cool the surface of the body.

To assess the potential cooling of the wall by the surface heat flux, it was assumed that the convective heat-transfer coefficient, h, corresponding to the data of Fig. 16, was a function only of x and was constant with respect to time. The wing was idealized as a 1-in.-thick, adiabatic backface slab of stainless steel (this is equivalent to a symmetric 2-in.-thick slab), and it was assumed that the conduction heat transfer in the wing was locally one-dimensional in the direction normal to the surface. Under these assumptions the transient temperature response of the wing surface was determined using Chart 25 of Ref. 21. The results of these calculations are shown in Fig. 17. These data show that after only 1 to 2 seconds of flow the surface is cooled to a $(T_w/T_o)_\infty$ value of approximately 1.035; however, the results presented in Section 3.1 indicate that even this variation from the adiabatic wall condition yields a potentially significant variation in turbulent boundary-layer parameters. Furthermore, although the case for which Fig. 17 applies is not one with boundary-layer separation, it does indicate that the flow on the surface has its least cooling influence near the trailing edge, where separation will first occur. Additionally, Fig. 17, taken with the other results presented in this section and the previous section, indicates that the variation of wall temperature with time over the duration of a 2- to 10-sec testing period would have surface temperature variations large enough that, with all other parameters held constant, the data taken within the testing period would not be self-consistent. These finds have important implications relative to HIRT testing in the sweeping pitch mode, where the model may be pitched at rates up to a maximum of 7.5 deg/sec during test times on the order of 2 to 3 seconds. Unsteady airfoil aerodynamic phenomena such as dynamic stall may be highly sensitive to rapidly changing temperature levels. More research needs to be done in this area of wall temperature effects on unsteady aerodynamics dominated by boundary-layer phenomena.

3.3 YAWED AIRFOIL IN MACH 0.815 HIRT FLOW

In order to assess the effects of wall temperature on the three-dimensional compressible turbulent boundary layer under HIRT conditions relative to flight, infinite yawed wing calculations of the sort discussed in Section 2.2 have been performed for the upper surface of the Douglas Aircraft Company (DAC) 30-deg-sweep airfoil given in Fig. 15 of Ref. 22; the free-stream conditions are identical to those of Section 3.2, which are representative of the HIRT facility as well as flight.

Shown in Fig. 18 are the inviscid flow parameters over the surface of the DAC airfoil. As can be seen from the figure, the chordwise (x-direction) inviscid flow is supercritical (local x-direction Mach number exceeds the sonic or critical value) while the spanwise (z-direction) inviscid flow remains subsonic throughout. For the present study the chordwise inviscid supercritical flow is not allowed to terminate via a shock wave but is forced to recompress smoothly over the aft section of the airfoil with a continually increasing adverse pressure gradient; this is done in order to assess the effects of continuous adverse pressure gradient on three-dimensional transonic turbulent boundary-layer flow. Note from Fig. 18 that the airfoil chord length is 1 ft, which is representative of allowable model size in the full-scale HIRT facility.

Figure 19 presents the distribution for the ratio of the adiabatic wall temperature to the free-stream total temperature. Note that this ratio ranges from 0.975 to 0.995 with a distribution almost identical to the two-dimensional case previously shown in Fig. 13. Also illustrated in Fig. 19 is the constant T_w = 540°R condition typical of HIRT conditions.

The effects of wall temperature on the three-dimensional turbulent skin-friction coefficients (both chordwise and spanwise) are given in Fig. 20. Both the chordwise and spanwise skin-friction coefficients under HIRT conditions are less than the corresponding location adiabatic wall values. This means that the integrated skin-friction drag on this airfoil under HIRT conditions would be smaller than the adiabatic wall drag on the same airfoil under identical free-stream conditions. As shown in Fig. 21, three-dimensional boundary-layer separation (defined as in Section 2.2) occurs at 98.6-percent chord under HIRT conditions and at 99.45-percent chord under adiabatic wall conditions. These results are similar to those reported in Section 3.1 for two-dimensional airfoil flows with boundary-layer separation.

Figures 22 and 23 present the chordwise and spanwise shape factors, respectively, for the three-dimensional turbulent boundary layer on the DAC airfoil. Interpretation of the shape factor as a characteristic parameter of the turbulent boundary layer (see Ref. 2) in conjunction with the trends revealed by Figs. 22 and 23 indicates that the three-dimensional turbulent boundary-layer structure under HIRT conditions relative to adiabatic wall conditions deserves careful attention. Study of Fig. 24 shows that both the chordwise and spanwise displacement thicknesses under HIRT conditions are approximately 10 percent larger than the corresponding adiabatic wall values at a common location. Figure 25 shows, however, that the chordwise and spanwise momentum thicknesses

are almost identical under HIRT and adiabatic wall conditions. Since the displacement thickness is the key parameter governing viscous-inviscid interaction phenomena, these results indicate a potential problem in interpretation of HIRT experimental data relative to flight under flow situations where viscous-inviscid interactions are important (and perhaps dominant, as in shock/boundary-layer interaction under transonic conditions). One important point relative to interpretation of the chordwise and spanwise displacement thicknesses is that it is only the chordwise value (δ_x^*) which has physical meaning on an infinite yawed wing. (See the classic report by Moore (Ref. 23) for a complete discussion of three-dimensional boundary-layer displacement thicknesses and their interpretation.)

The surface and external (inviscid) flow angle distributions over the DAC airfoil are presented in Figs. 26 and 27. Note the large amount of boundary-layer turning under the external (inviscid) flow near the trailing edge of the airfoil. As can be seen from these figures, there is little difference in surface flow angle forward of the 90-percent chord location between the HIRT and adiabatic wall conditions; the major difference occurs close to boundary-layer separation, as may be expected based on the results of Fig. 21. These findings reveal that the direction of the surface shear stress on a yawed airfoil under HIRT conditions is essentially the same as it is under adiabatic wall conditions - an important result relative to interpretation of force and moment data on yawed airfoils under HIRT conditions.

The surface heat-transfer distribution on the yawed DAC airfoil under HIRT conditions is given in Fig. 28. Comparison of Fig. 28 with Fig. 16 for the case of two-dimensional flow reveals that the distributions are almost identical, so that all of the findings of Section 3.2 concerning surface heat transfer from the two-dimensional airfoil to the boundary layer apply without change to the present three-dimensional case.

3.4 YAWED AIRFOIL IN MACH 0.815 HIRT FLOW UNDER HOT-WALL CONDITIONS TYPICAL OF SHUTTLE ENTRY

With the advent of maneuverable reentry vehicles such as the Space Shuttle, a new problem involving heat transfer from hot aerodynamic surfaces has evolved. During reentry into the atmosphere, the Shuttle will be subjected to large heat loads which depend upon the geometric configuration as well as the attitude of the vehicle during reentry. Some of this entry heat load will inevitably soak into the structure and aerodynamic

surfaces. After the hypersonic reentry phase of the flight, the Shuttle will slow to subsonic speeds and maneuver for a conventional aircraft landing. It has been estimated by NASA (see Ref. 24) that the Shuttle wings may reach soak temperatures on the order of 1000°R, which is some 2.5 times the local free-stream stagnation temperature under subsonic flight conditions. Thus, during the transonic maneuvering and subsonic landing phase of Shuttle reentry, the heated aerodynamic surfaces will be (literally) injecting heat into a high Reynolds number turbulent boundary layer. The important question relative to transonic testing of Shuttle vehicles becomes, "What are the aerodynamic effects of high rates of heat transfer from the surface to a transonic, turbulent boundary layer, and must we simulate this hot-wall environment in ground testing of Shuttle configurations?"

In order to provide some insight into the above-defined problem area, to which little or no attention has been given in previous VKF studies, the 30-deg-sweep infinite yawed airfoil calculations of Section 3.3 have been repeated assuming a constant surface temperature of 1000°R over the entire wing. All other parameters (free-stream conditions, wing pressure distribution, etc.) have been held fixed at the full-scale HIRT conditions of Section 3.3, namely

$$M_\infty = 0.815$$

$$Re_{\infty, c} = 1.05 \times 10^8$$

which are very close to actual flight values quoted in Fig. 3 of Ref. 25 for the McDonnell Douglas Astronautics Company (MDAC) Shuttle Orbiter at an altitude of 42,500 feet. In all of the calculated results to be presented below, hot-wall (constant surface temperature of 1000°R over the entire wing) results typical of actual Shuttle entry conditions will be compared with adiabatic-wall results since an adiabatic-wall condition represents conventional transonic testing in continuous wind tunnels such as the AEDC Propulsion Wind Tunnel (16T) and Aerodynamic Wind Tunnel (4T).

Figures 29 through 33 present the results of the hot (1000°R)- versus adiabatic-wall calculations. As can be seen from Fig. 29, three-dimensional turbulent boundary-layer separation (defined as the surface location where $\omega_s \equiv 0$) occurs at 93-percent chord for the hot-wall case and 99-percent chord for the adiabatic-wall condition; note that over the entire aft half of the airfoil the adiabatic-wall surface flow angle is always larger than the corresponding x-location hot-wall value. The x-

and z-direction components of the three-dimensional turbulent skin-friction coefficient are presented in Fig. 30, the important point being that the hot wall reduces the local x-direction skin friction by some 20 to 40 percent over the corresponding location x-direction adiabatic-wall value. Similarly, the z-direction hot-wall skin friction is reduced some 20 to 25 percent over the entire airfoil as compared with the corresponding location z-direction adiabatic-wall value. Needless to say, this significant decrease in local skin friction because of the heated wall can result in appreciable reduction of integrated skin-friction drag on the airfoil. The corresponding calculated three-dimensional turbulent boundary-layer parameters (H, δ^*, θ_m) for both the x- and z-directions are presented in Figs. 31 through 33. Note from Fig. 31 the sizable increase in the shape factors H_x and H_z caused by the heated wall as compared with the adiabatic wall. The reason for this behavior can be seen from Figs. 32 and 33, where in general, the hot wall increases the displacement thicknesses, δ_x^* and δ_z^*, over the entire airfoil but decreases the momentum thicknesses, $\theta_{m,x}$ and $\theta_{m,z}$, over the majority of the airfoil. Recalling from Section 3.3 that it is the x-direction displacement thickness, δ_x^*, which has physical meaning relative to infinite yawed wing boundary-layer interaction with the inviscid flow, one may note that Fig. 32 shows that the hot wall increases the magnitude of δ_x^* some 50 percent over the entire airfoil as compared with the corresponding x-location adiabatic-wall value.

All of the above-presented results clearly indicate that hot-wall effects can indeed have a significant influence on transonic aerodynamics. The recent experimental investigation of Ref. 24 conducted in the Texas A&M University 7- by 10-ft subsonic wind tunnel using an electrically heated NACA 0012-64 airfoil reveals that both the maximum lift coefficient, $C_{L_{max}}$, and the stall angle of the airfoil, α_{stall}, are reduced as the wing-to-free-stream temperature ratio, T_w/T_∞, is increased under subsonic conditions; the following statistics illustrate this fact.

T_w/T_∞	$C_{L_{max}}$	α_{stall}
1.0	1.6	17.0
2.0	1.2	
2.2		12.5

Hence, simulation of the hot-wall/cold free-stream environment using electrically heated models appears necessary in ground testing under subsonic and transonic conditions for Shuttle applications, especially for aerodynamic drag and stall characteristics. More work, both analytical and experimental, is definitely needed to fully explore and understand this relatively new area of hot-wall subsonic and transonic aerodynamics for application to lifting bodies such as the Space Shuttle. Especially desirable for future studies are turbulent boundary-layer structure measurements in two- and three-dimensional subsonic and transonic flows under controlled hot-wall conditions.

SECTION IV
CONCLUDING SUMMARY

To provide the data necessary for prediction of full-scale transonic aircraft performance requires not only that wind tunnel data be obtained at the highest possible Reynolds number, but that we understand the effects of turbulent boundary-layer parameters on the resulting aerodynamic data. The present report considers one aspect which has received little or no attention in previous studies, namely wall temperature effects on the two- and three-dimensional turbulent boundary layer under VKF HIRT conditions ($T_w > T_{o,\infty}$) relative to flight ($T_w = T_{aw} < T_{o,\infty}$); also considered are hot-wall conditions ($T_w \approx 2T_{o,\infty}$) relative to Space Shuttle transonic flight during entry.

Numerical calculations for representative two- and three-dimensional transonic airfoil flows under HIRT conditions reveal that the high Reynolds number turbulent boundary layer is indeed sensitive to wall temperature. Standard operation of the HIRT facility with an initial model temperature of 540°R appears undesirable in that it results in an increase (or mismatch) of about 11 percent in terms of wall-to-stagnation temperature ratio relative to the adiabatic-wall ratio; the effects of this mismatch on resulting boundary-layer and aerodynamic parameters are larger than the influence of a decrease in the free-stream Reynolds number of almost 13 percent, holding the wall adiabatic. Furthermore, the present study indicates that the model wall temperature will be rapidly changing during a typical HIRT testing period of from 2 to 10 sec if the model is initially at 540°R; this may be undesirable for HIRT testing in the sweeping pitch mode since unsteady aerodynamic phenomena (e.g., airfoil dynamic stall) can be highly sensitive to rapidly changing turbulent boundary-layer wall temperature levels. One solution to this potential problem

is simply to precool the model to the free-stream stagnation temperature before initiation of the HIRT flow.

Ground testing of Space Shuttle configurations under continuous transonic flow conditions with an adiabatic wall may not be totally applicable to actual Shuttle entry, where the wing surface temperature may reach soak values on the order of twice the free-stream stagnation temperature due to the hypersonic high heating phase of the reentry trajectory. Numerical calculations presented in the present report indicate an appreciable reduction of integrated skin-friction drag on a hot-wall ($T_w/T_{0,\infty} \approx 2$) airfoil relative to the same airfoil under adiabatic wall conditions. Airfoil static stall angle and maximum lift coefficient, as well as turbulent boundary-layer parameters, are strongly affected by hot-wall relative to adiabatic-wall conditions. Hence, simulation of the hot-wall/cold free-stream environment using electrically heated models appears necessary in ground testing under continuous subsonic and transonic wind tunnel conditions for Space Shuttle applications, especially for aerodynamic drag and stall characteristics determination.

The present work makes no attempt to address the problem of wall temperature effects on viscous-inviscid interactions at transonic speeds; the term viscous-inviscid interaction is taken here to embrace all flow situations in which the development of the boundary layer and wake has a significant effect on the pressure field. An excellent discussion of this topic may be found in the recent report by Green (Ref. 26) for the case of adiabatic wall transonic flows.

A recent paper entitled "Delta Wing Separation Can Dominate Shuttle Dynamics," by Reding and Ericsson (Ref. 27), examines the unsteady aerodynamics of the delta wing Space Shuttle Orbiter. With respect to transonic aerodynamics of the delta-wing configuration, one major problem area involves sudden leading-edge stall, whereby boundary-layer separation can suddenly switch from the transonic shock-induced variety to leading-edge separation with a corresponding discontinuous change in wing loading. Further, a mixed-flow condition can result on the (swept) delta wing whereby the inner portion of the wing may be stalled at the leading edge while the flow over the outer wing leading edge is attached, with shock-induced separation a short distance downstream. In the unsteady case the demarcation line between these two flow conditions will oscillate spanwise as the wing pitches or plunges. The important question remains as to how wall temperature affects the above-defined unsteady transonic aerodynamic phenomena via the high Reynolds number turbulent boundary layer.

REFERENCES

1. Green, J. E., Weeks, D. J., and Pugh, P. G. "Some Observations Upon the Influence of Charge-Tube Mach-Number Upon the Utility of Flows Generated by Expansion Waves." Unpublished RAE Report, 1972.

2. Green, J. E. "Application of Head's Entrainment Method to the Prediction of Turbulent Boundary Layers and Wakes in Compressible Flow." RAE TR 72079, June 1972.

3. Starr, R. F. and Schueler, C. J. "Experimental Studies of a Ludwieg Tube High Reynolds Number Transonic Tunnel." AIAA Paper No. 73-212, presented at the AIAA 11th Aerospace Sciences Meeting, Washington, D. C., January 10-12, 1973.

4. Patankar, S. V. and Spalding, D. B. Heat and Mass Transfer in Boundary Layers. CRC Press, Cleveland, Ohio, 1968.

5. Mayne, A. W., Jr. and Dyer, D. F. "Comparisons of Theory and Experiment for Turbulent Boundary Layers on Simple Shapes at Hypersonic Conditions." Proceedings of the 1970 Heat Transfer and Fluid Mechanics Institute, Stanford University Press, Stanford, California, 1970, pp. 168-188.

6. Whitfield, D. L., Lewis, J. W. L., Williams, W. D., et al. "Specie Number Density, Pitot Pressure, and Flow Visualization in the Near Field of Two Supersonic Nozzle Banks Used for Chemical Laser Systems." AEDC-TR-73-11 (AD760132), May 1973.

7. Adams, J. C., Jr. and Martindale, W. R. "Hypersonic Lifting Body Windward Surface Flow-Field Analysis for High Angles of Incidence." AEDC-TR-73-2 (AD756499), February 1973.

8. Adams, J. C., Jr. "Numerical Calculation of the Subsonic and Transonic Turbulent Boundary Layer on an Infinite Yawed Airfoil." AEDC-TR-73-112, July 1973.

9. Launder, B. E. and Spalding, D. B. Lectures in Mathematical Models of Turbulence. Academic Press, Inc., New York, 1972.

10. Sivasegaram, S. and Whitelaw, J. H. "The Prediction of Turbulent, Supersonic, Two-Dimensional, Boundary-Layer Flows." The Aeronautical Quarterly, Vol. XXII, August 1971, pp. 274-294.

11. Nash, J. F. and Patel, V. C. Three-Dimensional Turbulent Boundary Layers. SBC Technical Books, Scientific and Business Consultants, Inc., Atlanta, Georgia, 1972.

12. Owen, P. R. and Randall, D. G. "Boundary Layer Transition on a Sweptback Wing." RAE Tech. Memo. No. Aero 277, May 1952.

13. Chapman, G. T. "Some Effects of Leading-Edge Sweep on Boundary-Layer Transition at Supersonic Speeds." NASA TN D-1075, September 1961.

14. Nash, J. F. and Tseng, R. R. "The Three-Dimensional Turbulent Boundary Layer on an Infinite Yawed Wing." The Aeronautical Quarterly, Vol. XXII, November 1971, pp. 346-362.

15. Hicks, J. G. and Nash, J. F. "The Calculation of Three-Dimensional Turbulent Boundary Layers on Helicopter Rotors." NASA CR-1845, May 1971.

16. Adams, J. C., Jr. "Implicit Finite-Difference Analysis of Compressible Laminar, Transitional, and Turbulent Boundary Layers along the Windward Streamline of a Sharp Cone at Incidence." AEDC-TR-71-235 (AD734535), December 1971.

17. Adams, J. C., Jr. "Finite-Difference Analysis of the Three-Dimensional Turbulent Boundary Layer on a Sharp Cone at Angle of Attack in a Supersonic Flow." AIAA Paper No. 72-186, presented at the AIAA 10th Aerospace Sciences Meeting, San Diego, California, January 17-19, 1972.

18. Adams, J. C., Jr. "Analysis of the Three-Dimensional Compressible Turbulent Boundary Layer on a Sharp Cone at Incidence in Supersonic and Hypersonic Flow." AEDC-TR-72-66 (AD743003), June 1972.

19. Escudier, M. P. "The Distribution of the Mixing Length in Turbulent Flows Near Walls." Mechanical Eng. Dept. Report TWF/TN/1, Imperial College, London, March 1965.

20. Van Driest, E. R. "On Turbulent Flow Near a Wall." Journal of the Aeronautical Sciences, Vol. 23, No. 11, November 1956, pp. 1007-1011, 1036.

21. Schneider, P. J. Temperature Response Charts. John Wiley and Sons, Inc., New York, 1963.

22. Kaups, K. and Keltner, G. "Laminar Compressible Boundary Layer on a Yawed Infinite Wing." Douglas Aircraft Company Report No. LB 32706, March 1967.

23. Moore, F. K. "Displacement Effect of a Three-Dimensional Boundary Layer." NACA TN 2722, June 1952.

24. Macha, J. M., Norton, D. J., and Young, J. C. "Surface Temperature Effect on Subsonic Stall." AIAA Paper No. 72-960, presented at the AIAA 2nd Atmospheric Flight Mechanics Conference, Palo Alto, California, September 11-13, 1972.

25. Fehrman, A. L. and Masek, R. V. "Study of Uncertainties of Predicting Space Shuttle Thermal Environment." Report MDC E0639, June 1972.

26. Green, J. E. "A Discussion of Viscous-Inviscid Interactions at Transonic Speeds." RAE TR 72050, May 1972.

27. Reding, J. P. and Ericsson, L. E. "Delta Wing Separation Can Dominate Shuttle Dynamics." AIAA Paper No. 72-976, Presented at the AIAA 2nd Atmospheric Flight Mechanics Conference, Palo Alto, California, September 11-13, 1972.

APPENDIX
ILLUSTRATIONS

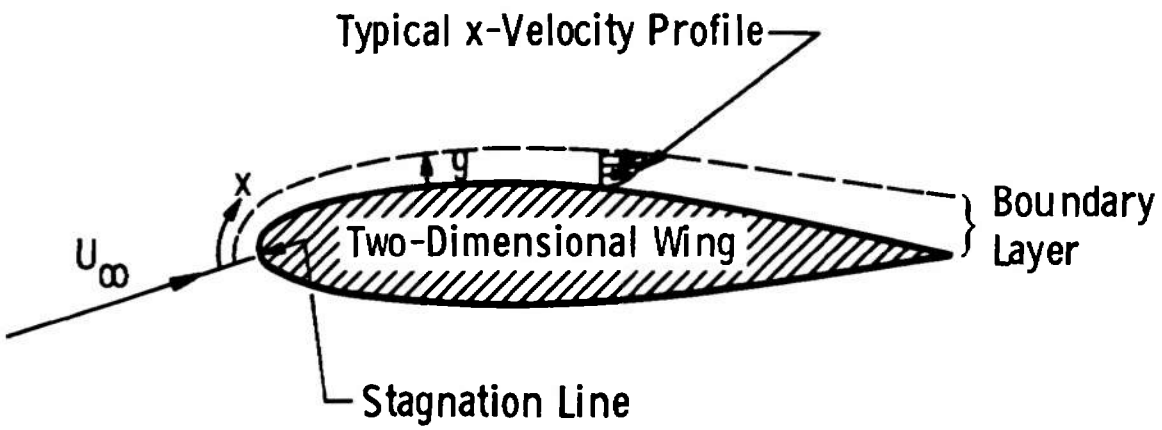

Fig. 1 Sketch of Flow Situation Indicating Some Primary Variables

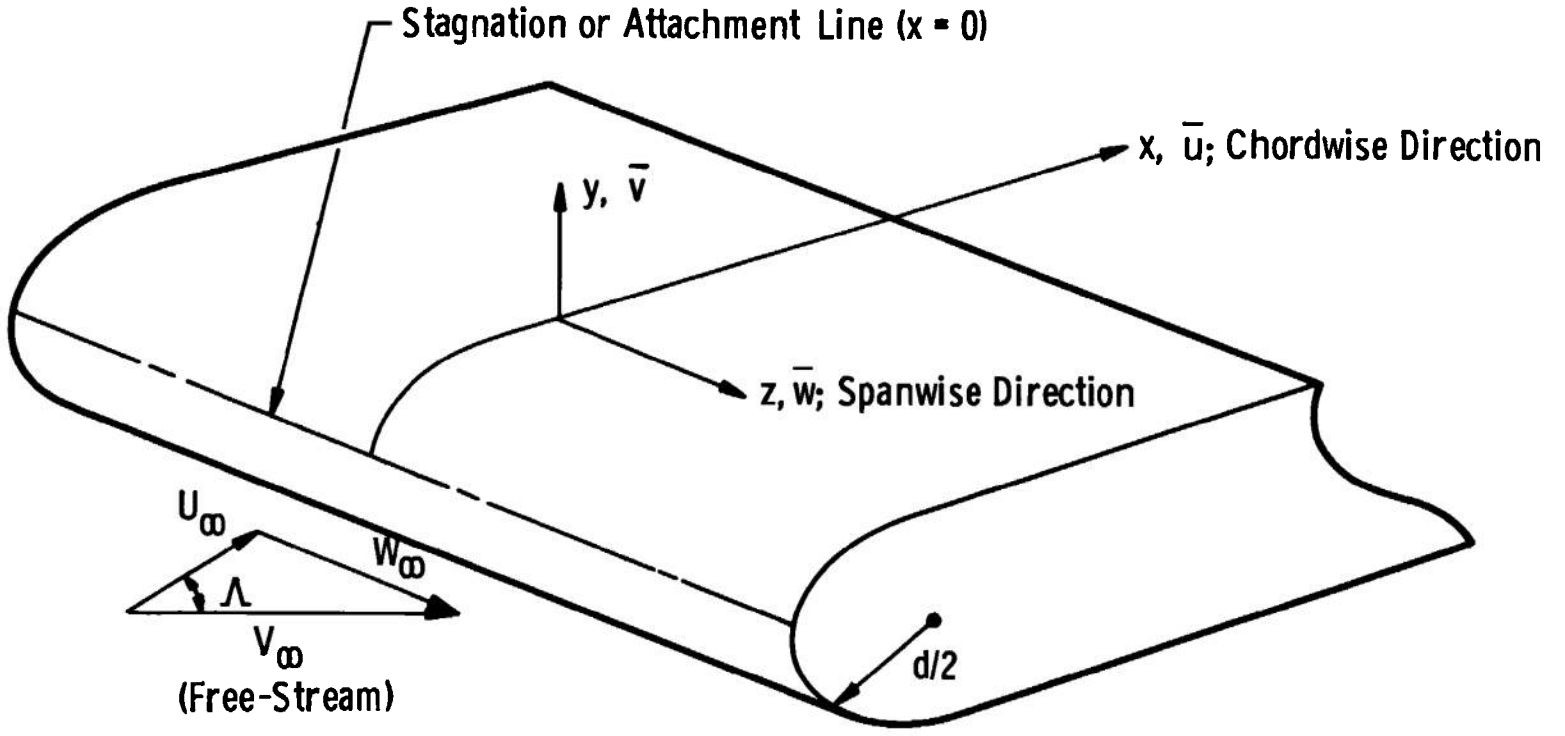

Fig. 2 Infinite-Extent Yawed Body Geometry and Nomenclature

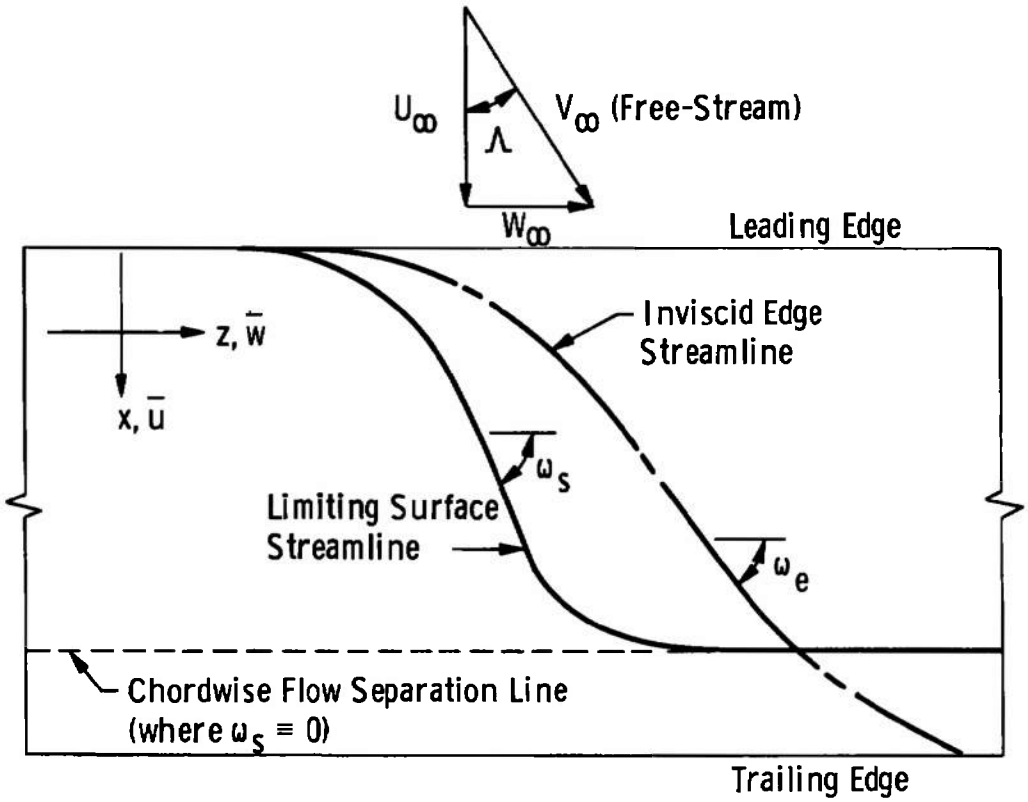

a. Plan View Illustrating Three-Dimensional Boundary-Layer Separation on an Infinite Yawed Wing

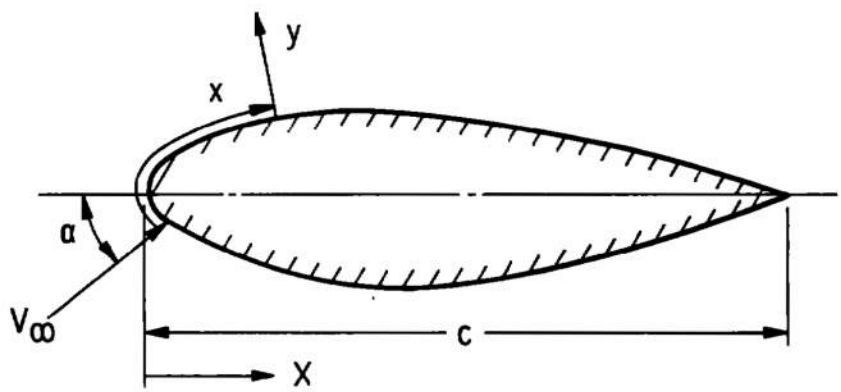

b. Chordwise Section of Wing

Fig. 3 Infinite Yawed Wing Geometry and Nomenclature

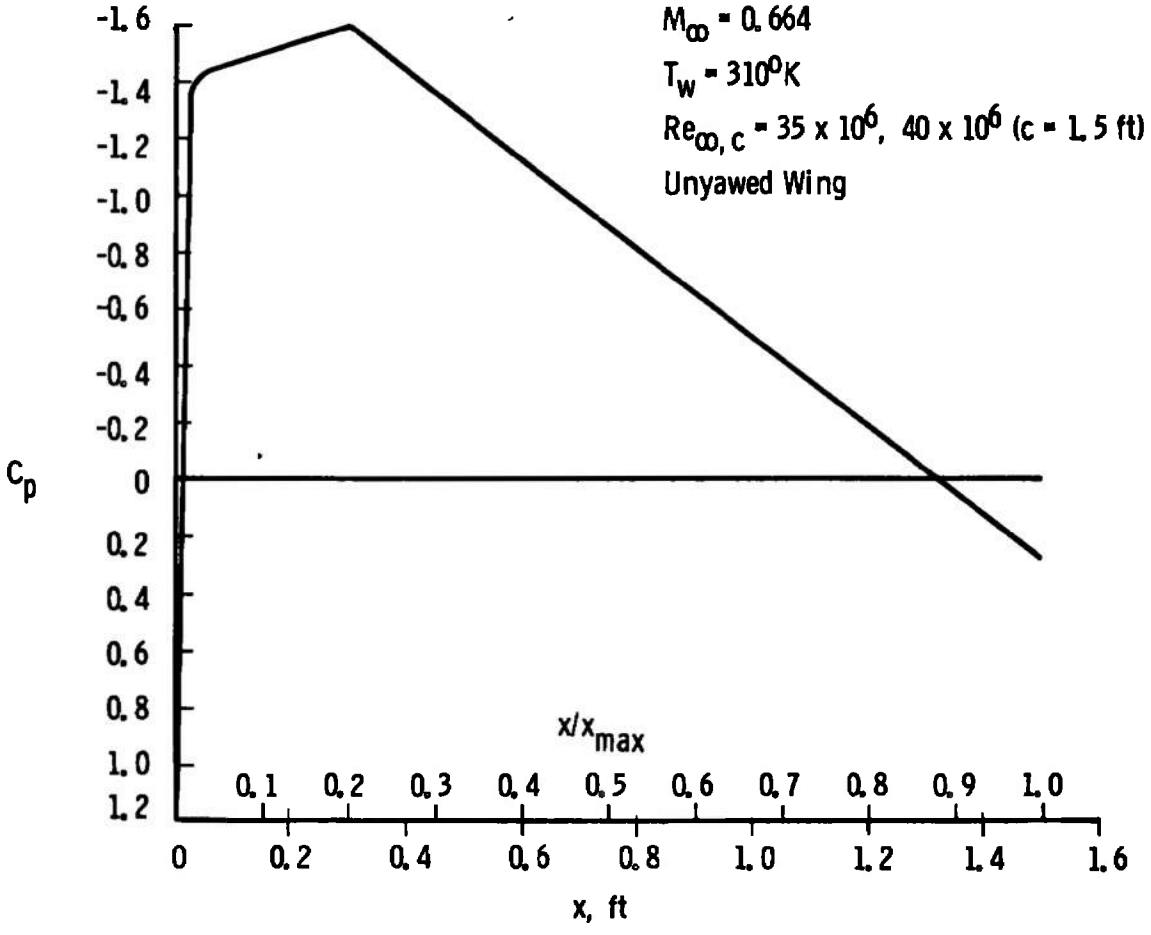

Fig. 4 C_p Used for Airfoil Wall Temperature Ratio Study (Similar to That Used by Green, Weeks, and Pugh, Ref. 1)

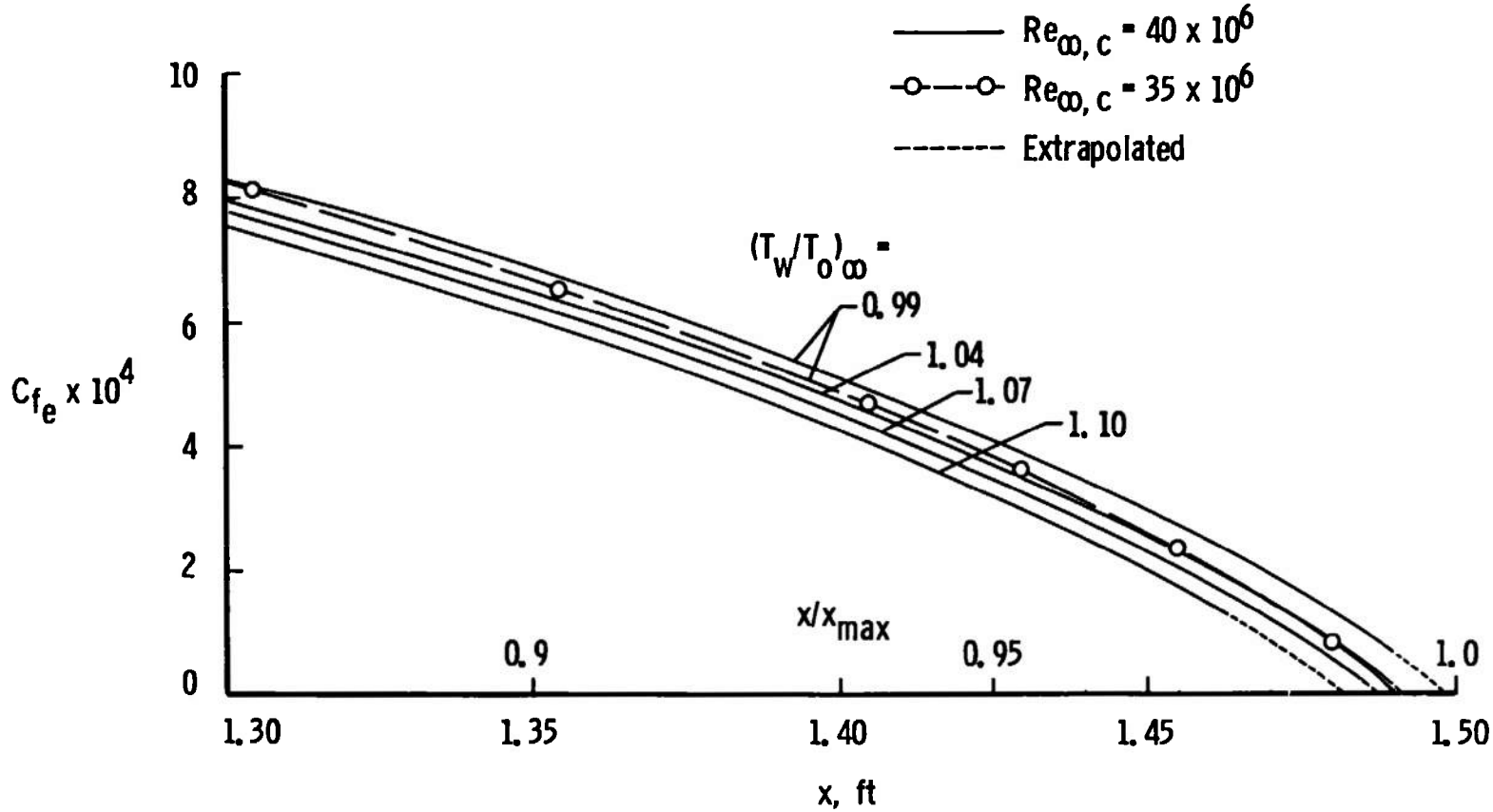

Fig. 5 Coefficient of Skin Friction

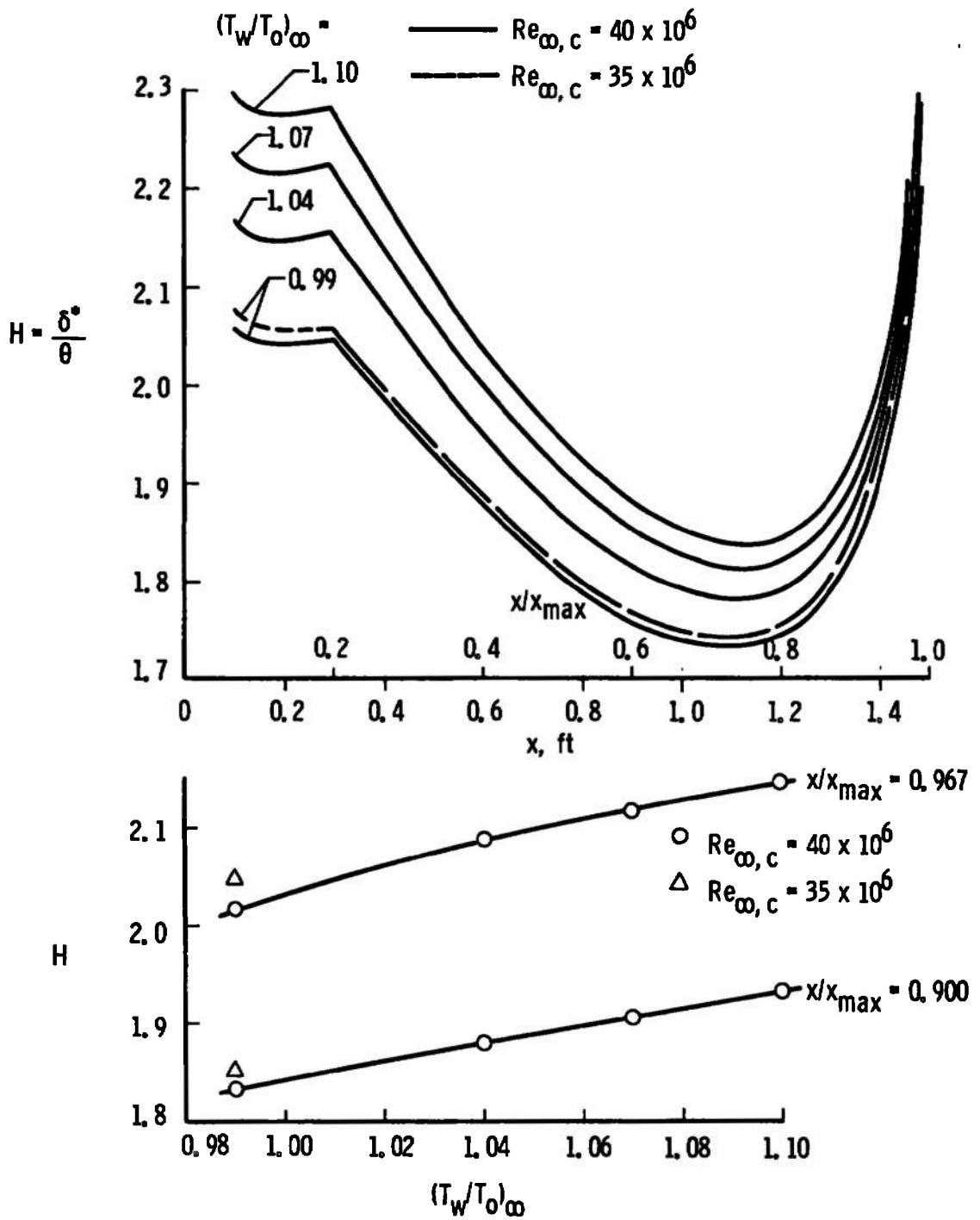

Fig. 6 Shape Factor

δ_0^* refers to case with $(T_w/T_0)_\infty = 0.99$ and $Re_{\infty,c} = 40 \times 10^6$.

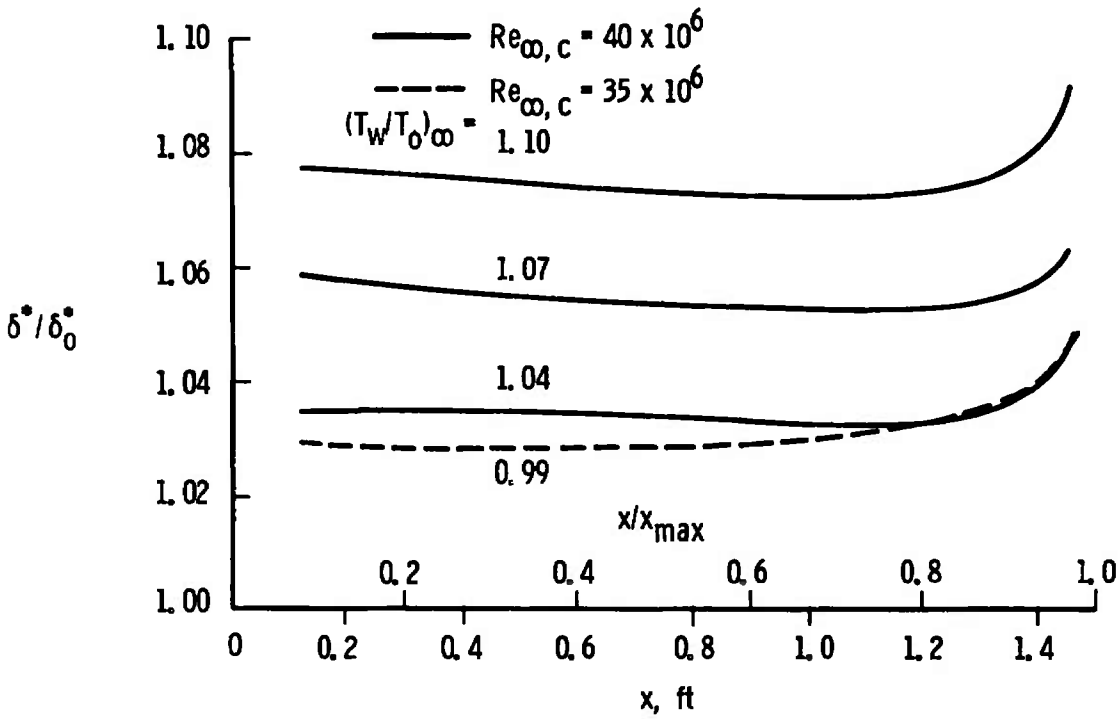

Fig. 7 Displacement Thickness Ratio

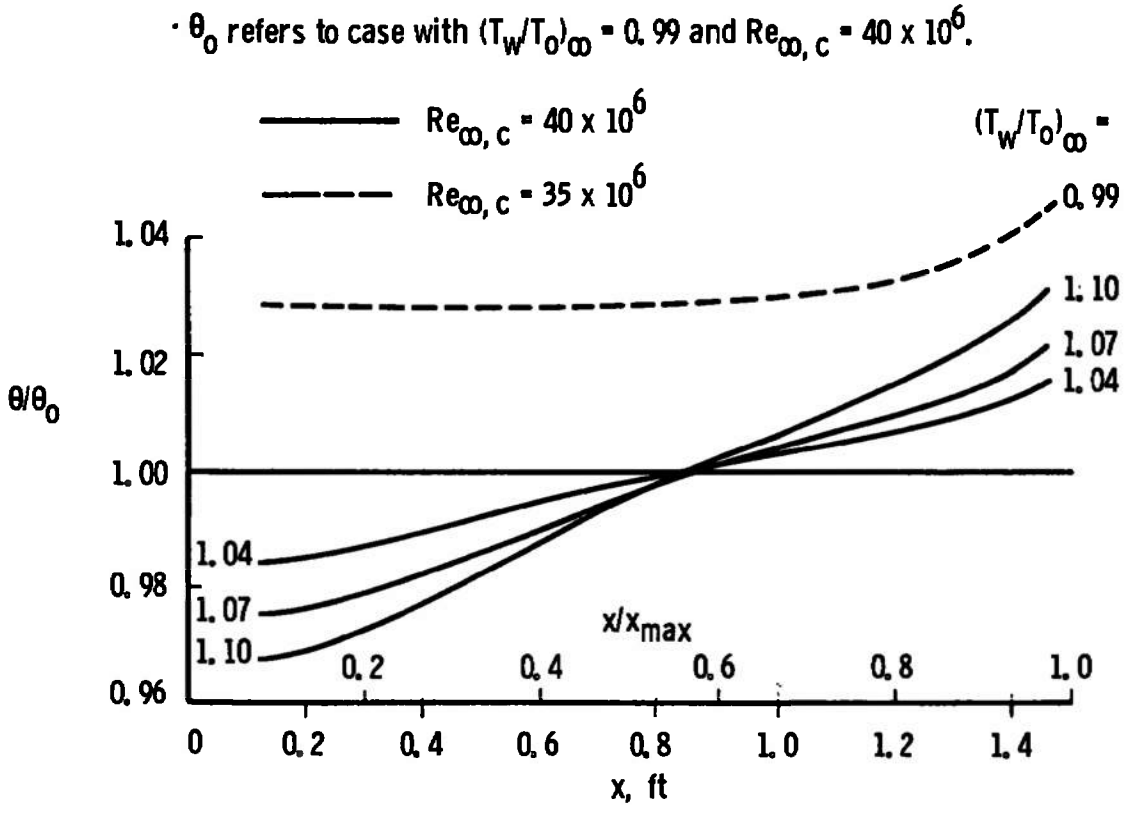

Fig. 8 Momentum Thickness Ratio

H_0 refers to case with $(T_w/T_0)_\infty = 0.99$ and $Re_{\infty,c} = 40 \times 10^6$.

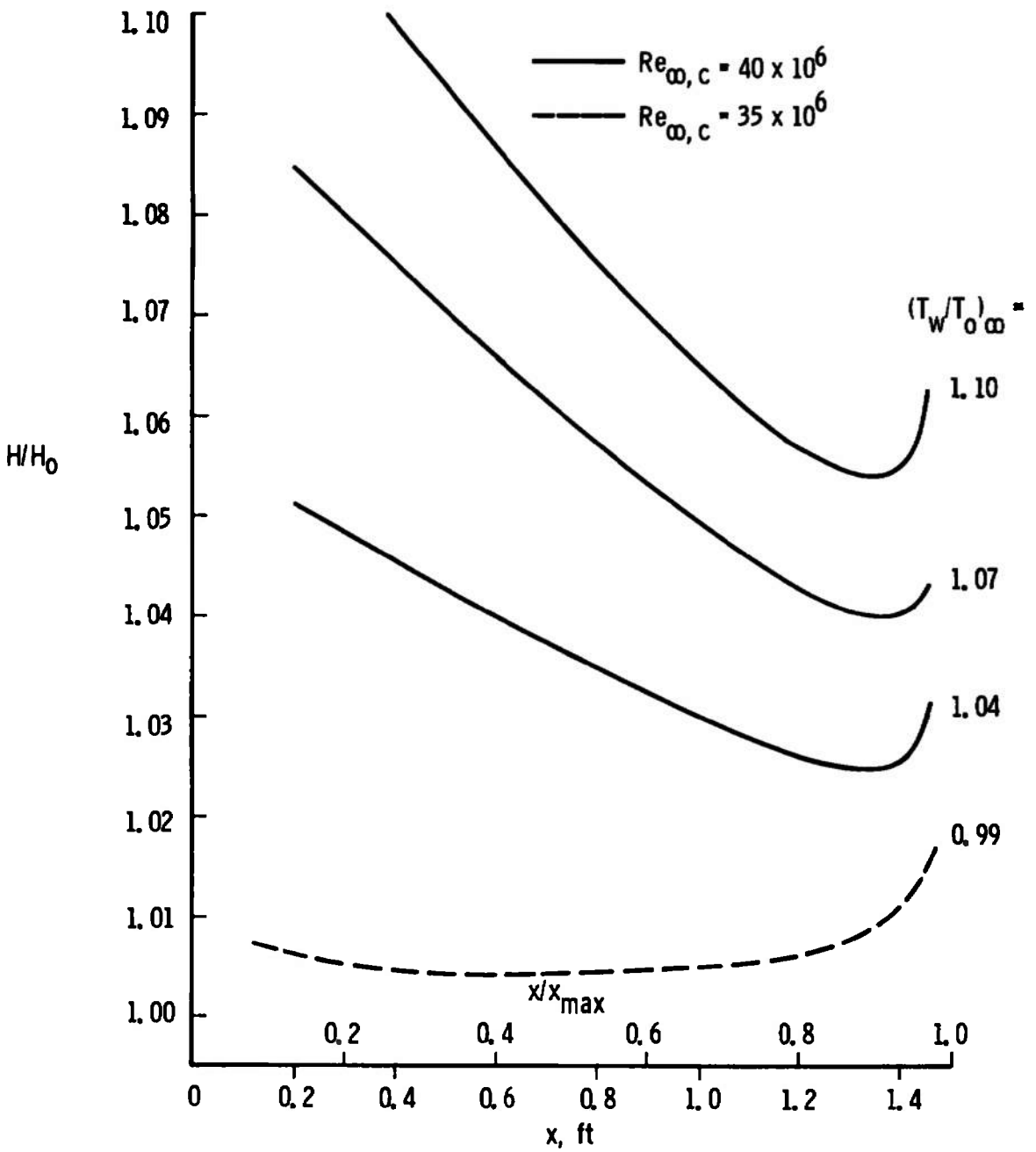

Fig. 9 Shape Factor Ratio

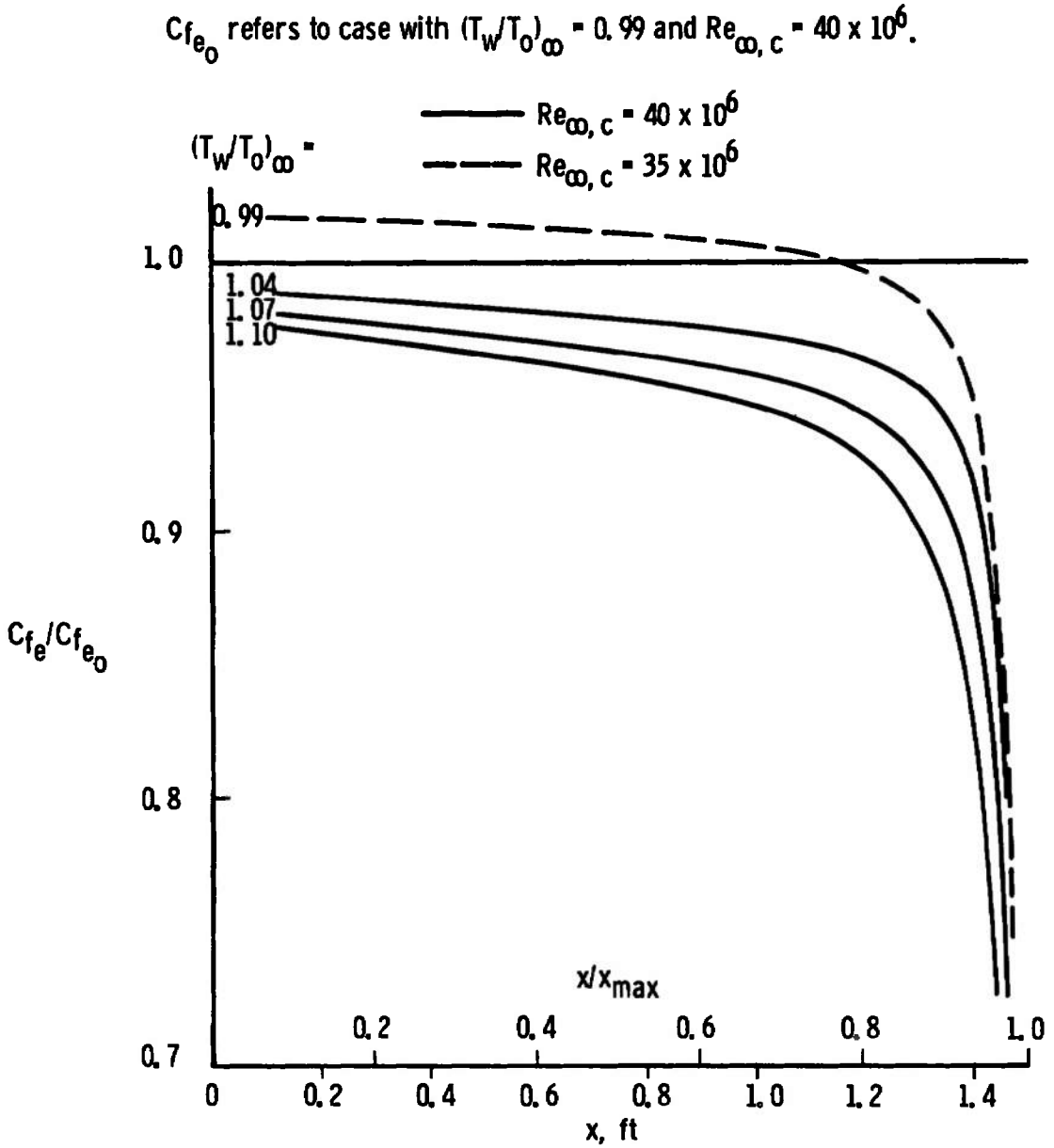

Fig. 10 Skin-Friction Coefficient Ratio

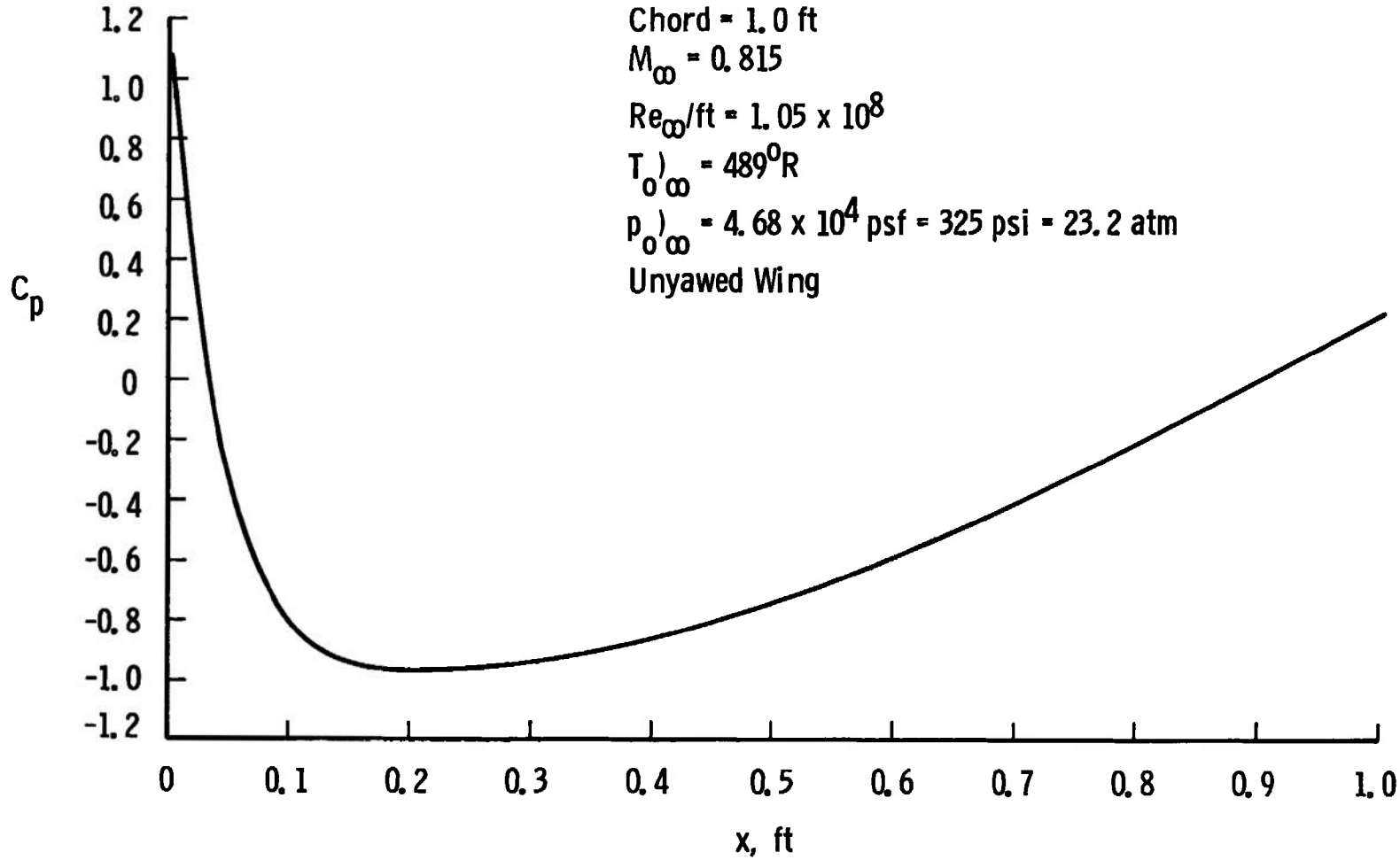

Fig. 11 Pressure Distribution for "Typical" Airfoil in HIRT

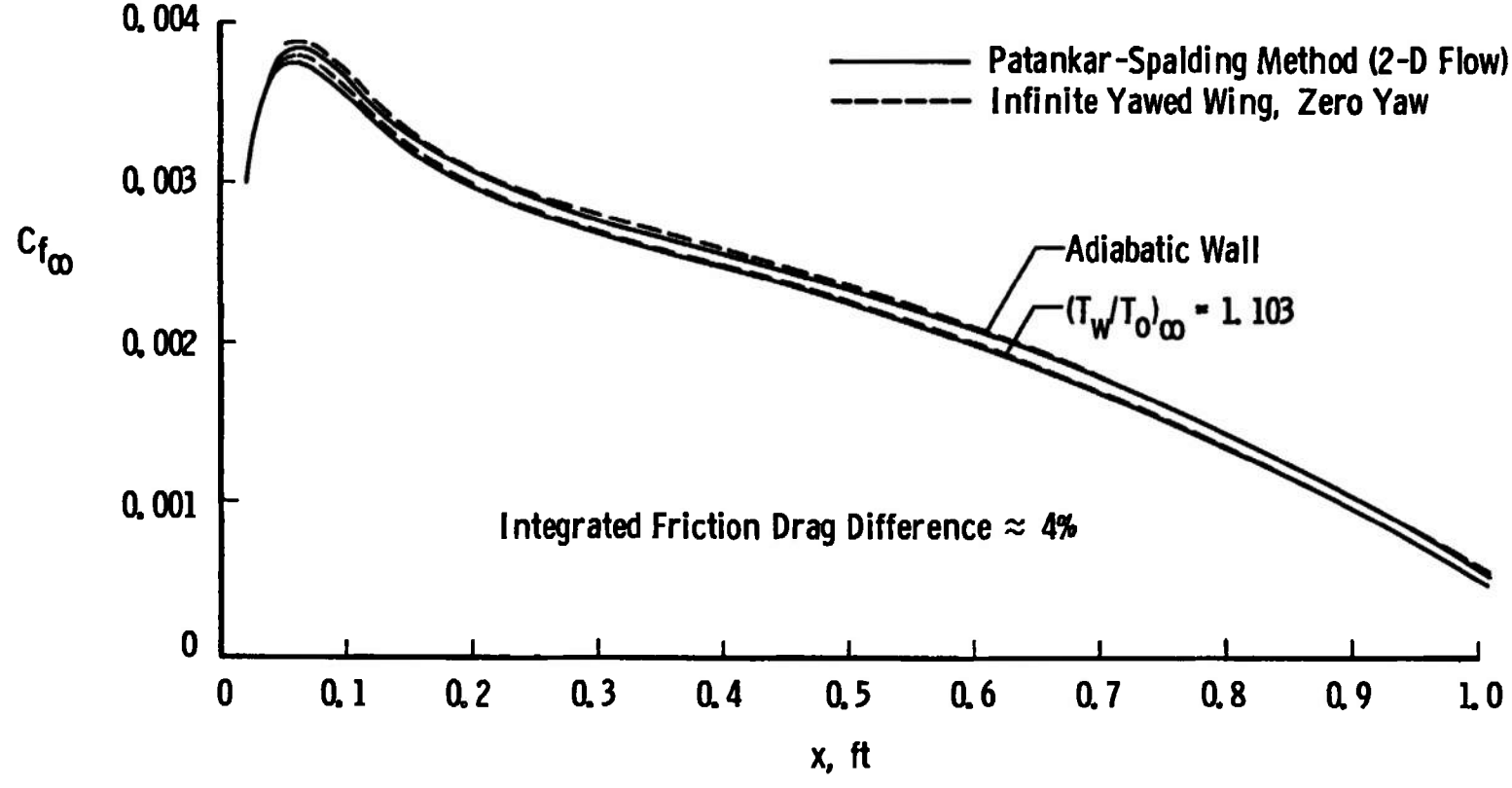

Fig. 12 Skin-Friction Coefficient over "Typical" Airfoil in HIRT

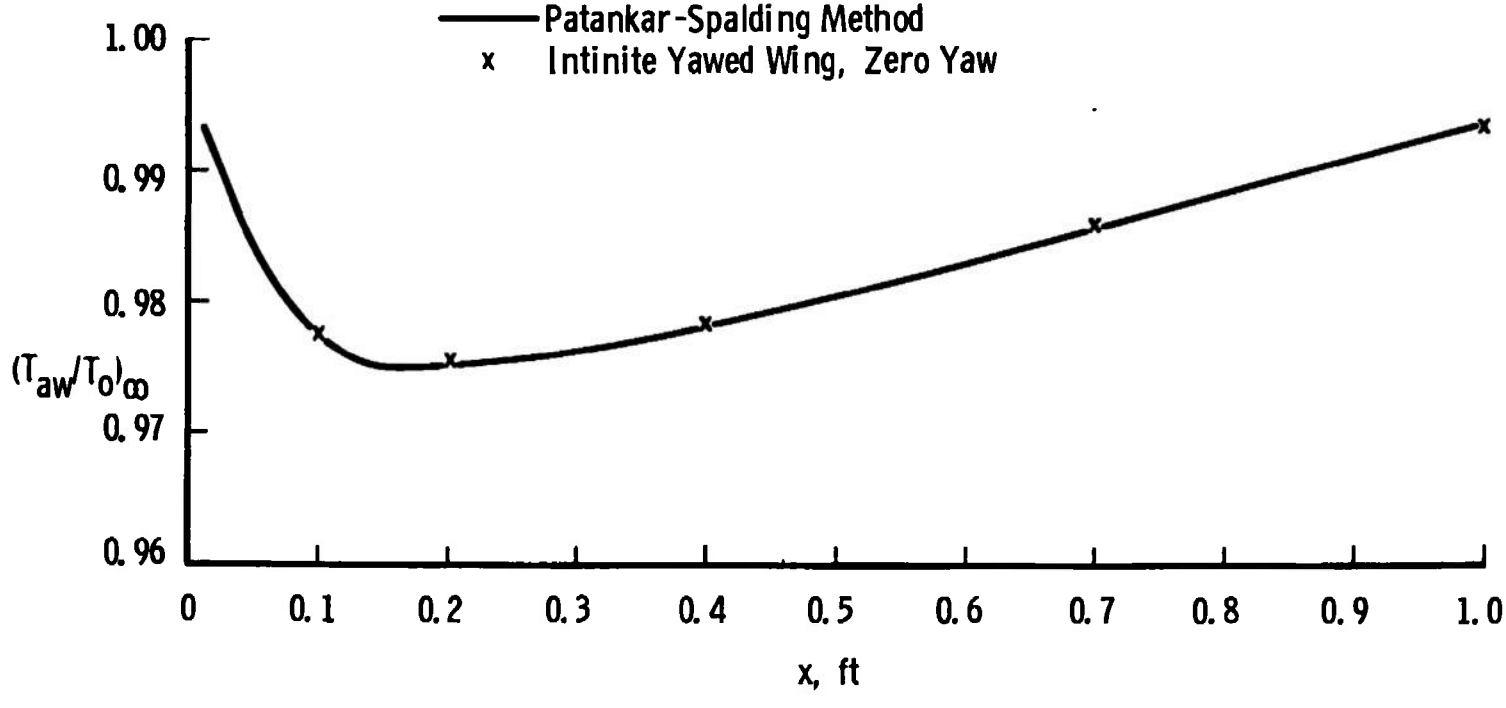

Fig. 13 Adiabatic Wall Temperature Ratio

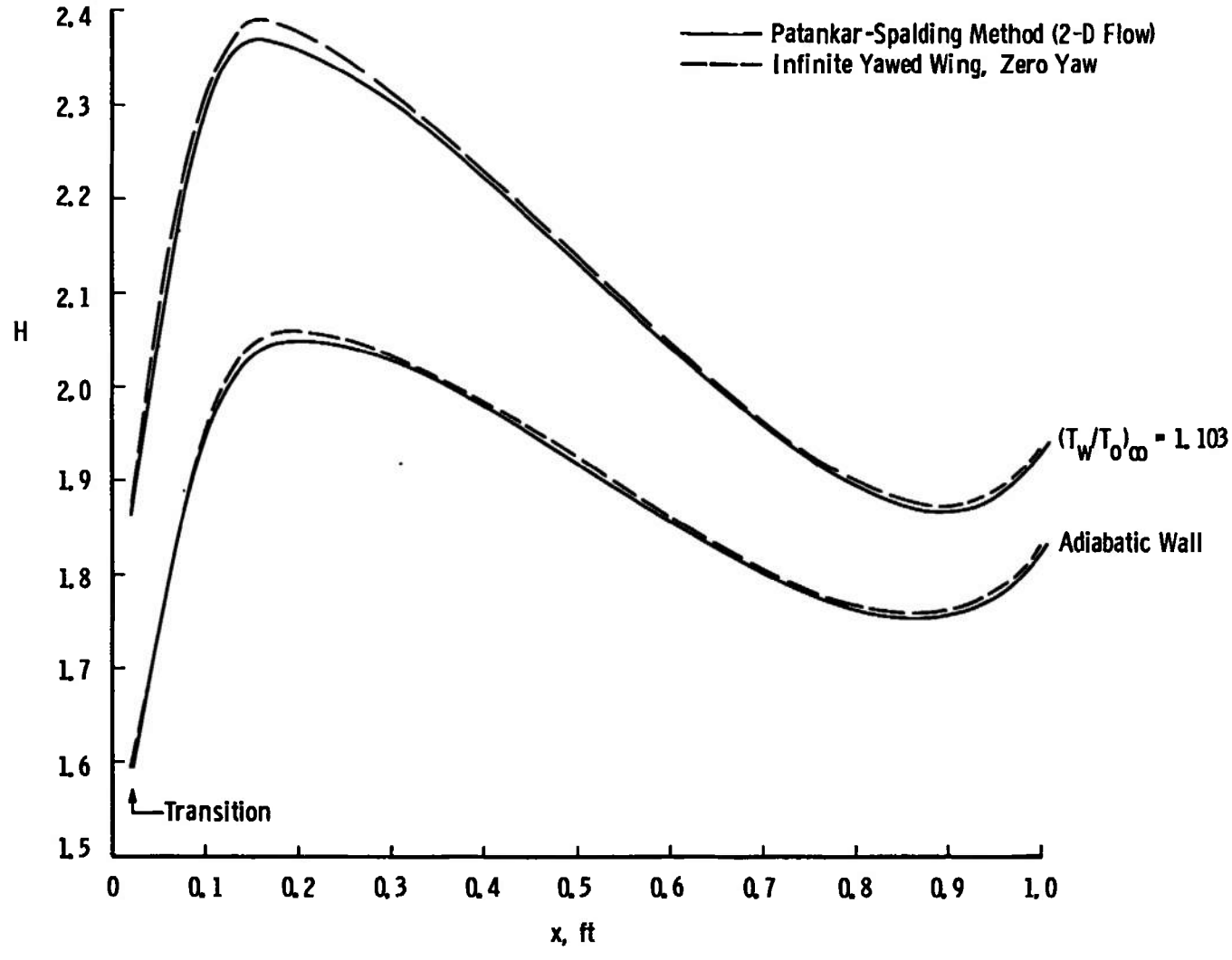

Fig. 14 Shape Factor over "Typical" Airfoil in HIRT

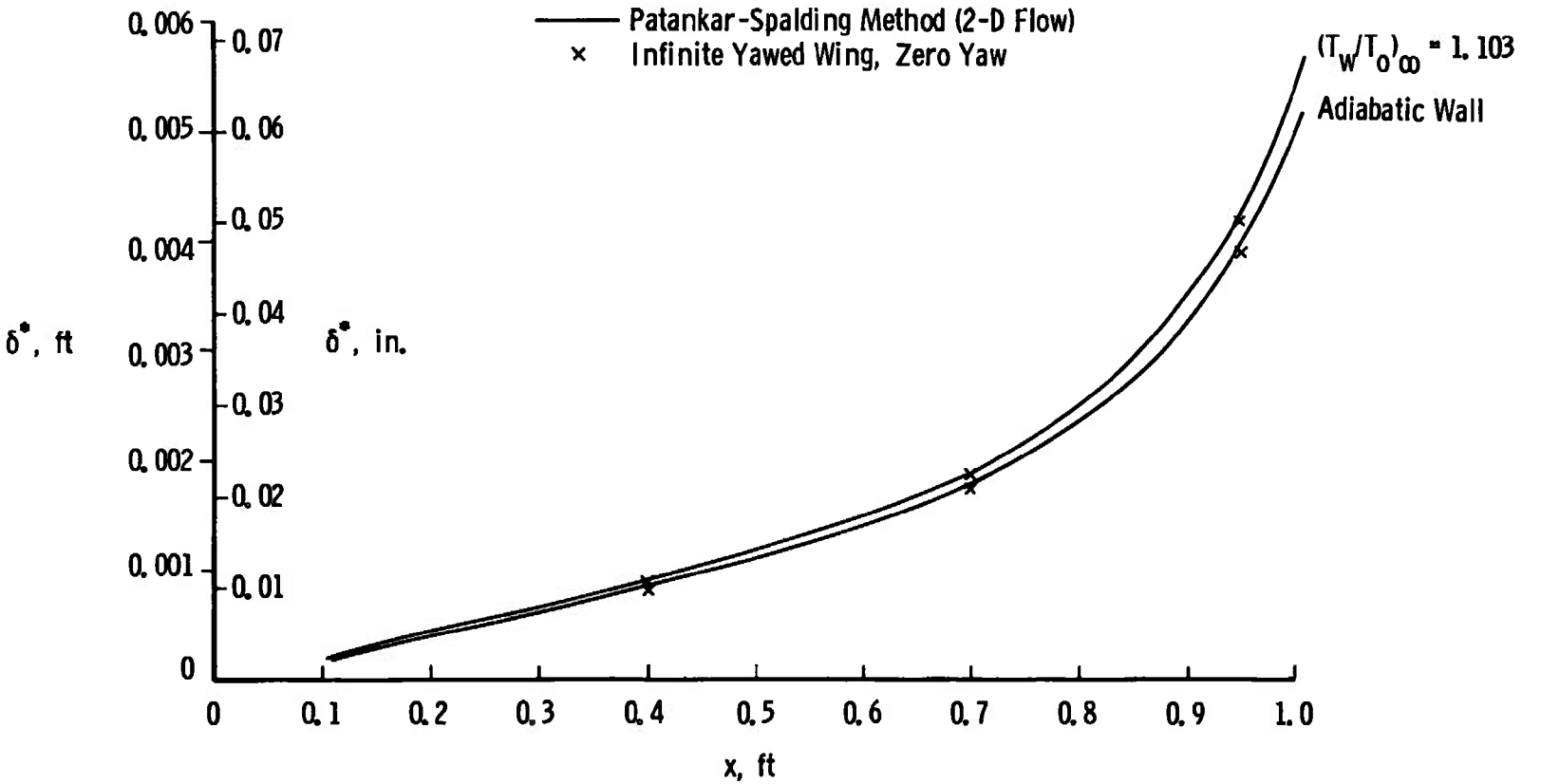

Fig. 15 Displacement Thickness over "Typical" Airfoil in HIRT

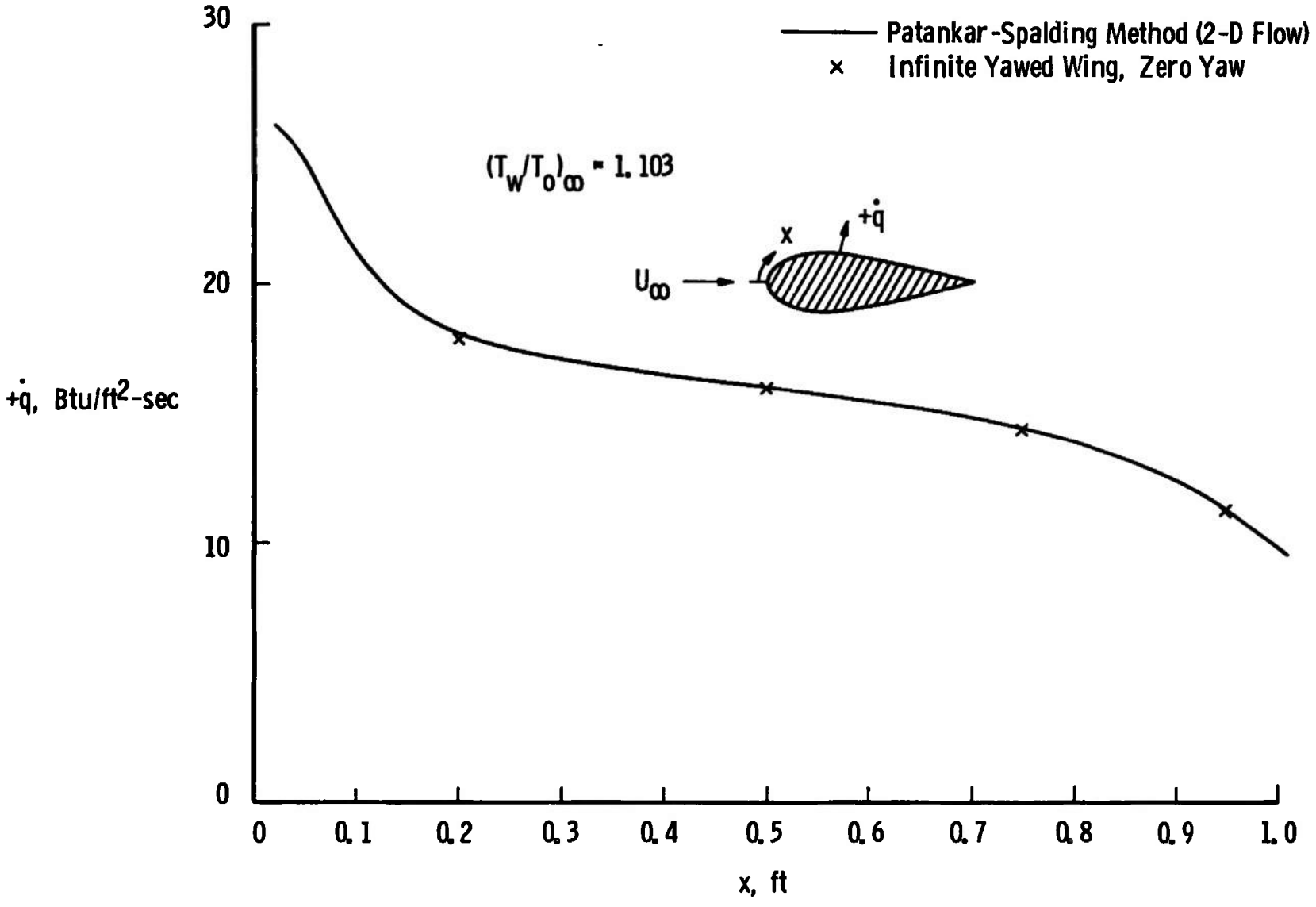

Fig. 16 Heat-Transfer Rate over "Typical" Airfoil in HIRT

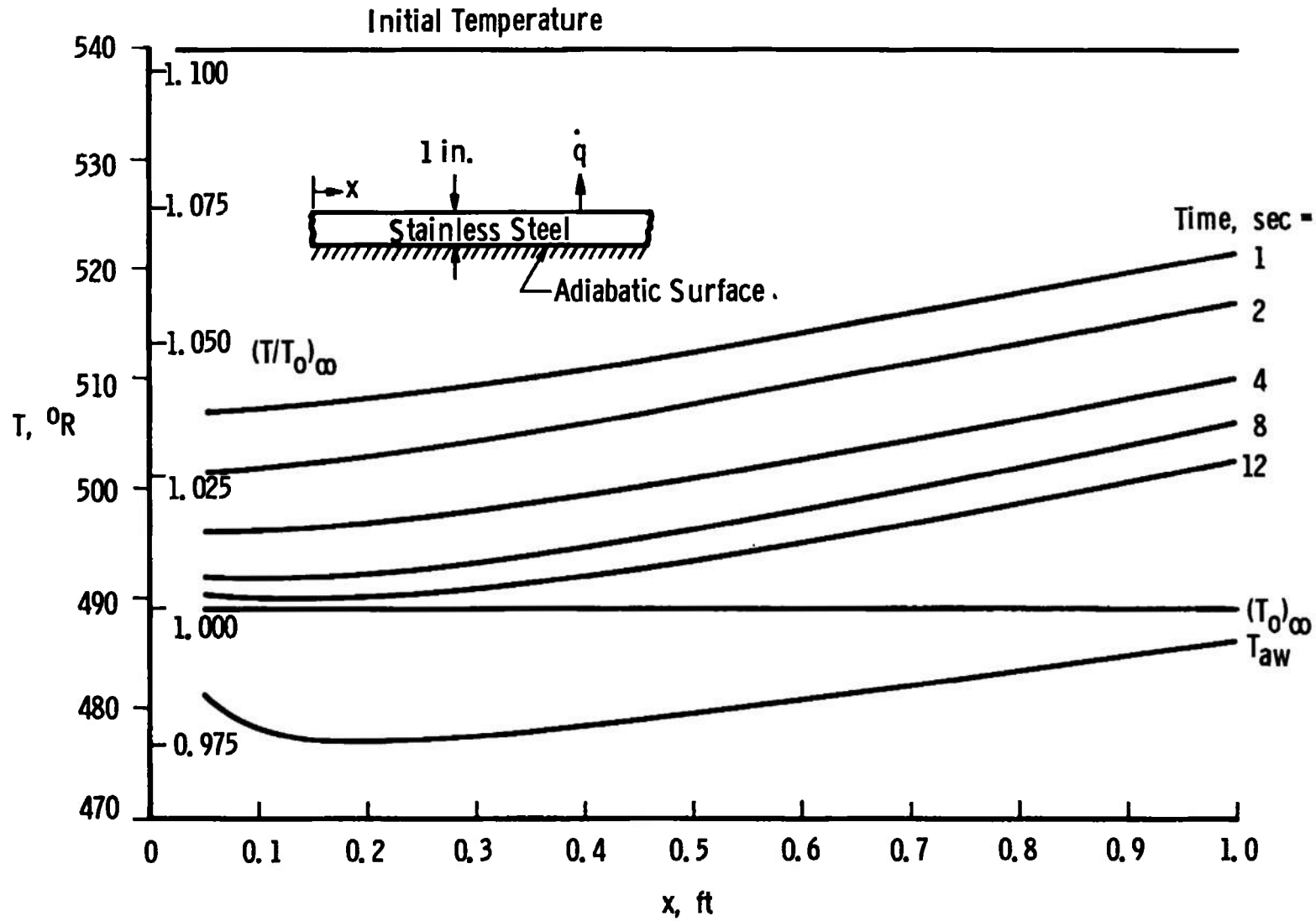

Fig. 17 Surface Temperature of 1-in.-Thick, Adiabatic Backface Slab

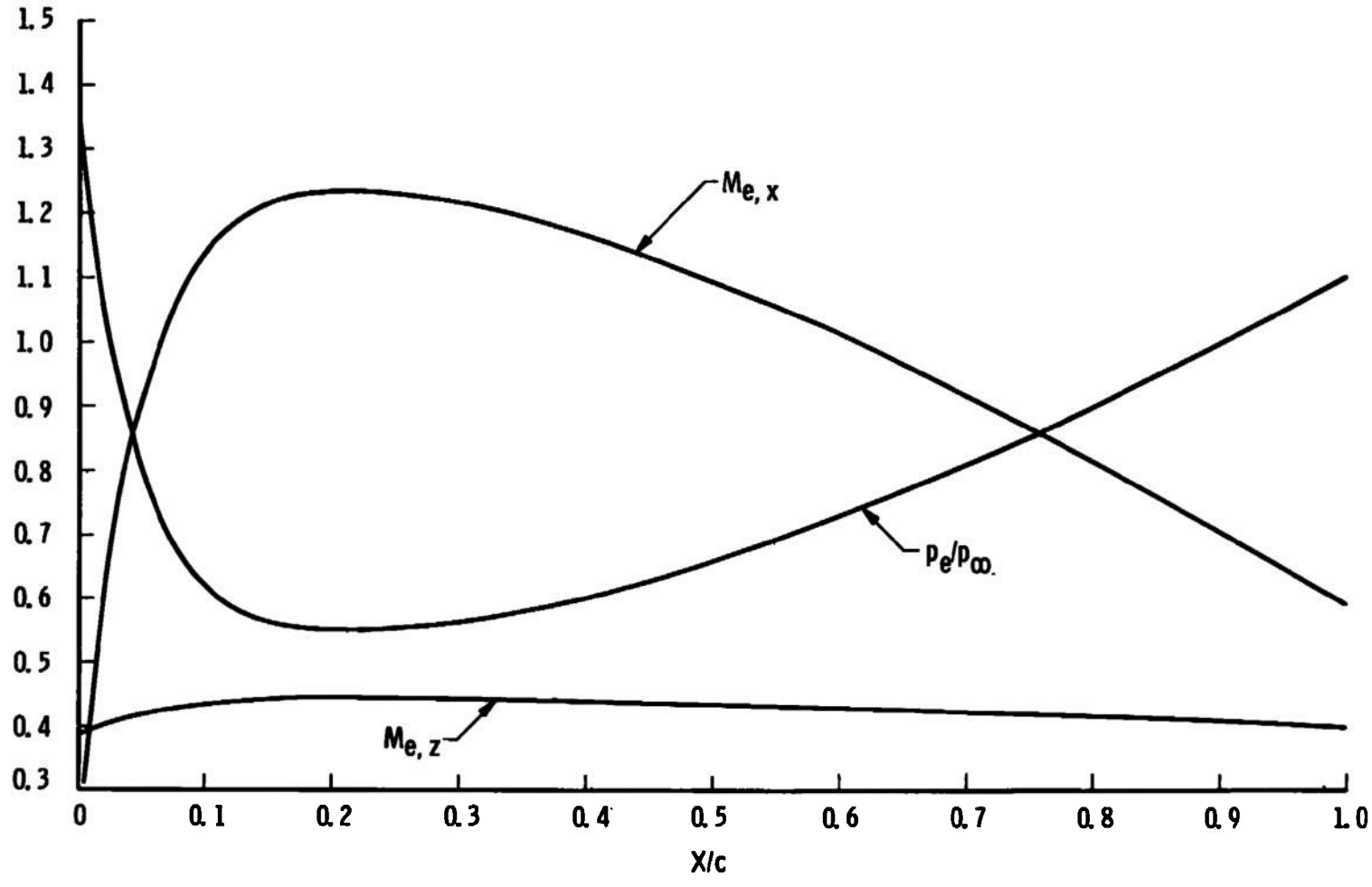

Fig. 18 Inviscid Flow Parameters on the DAC Airfoil Under Full-Scale HIRT Conditions.

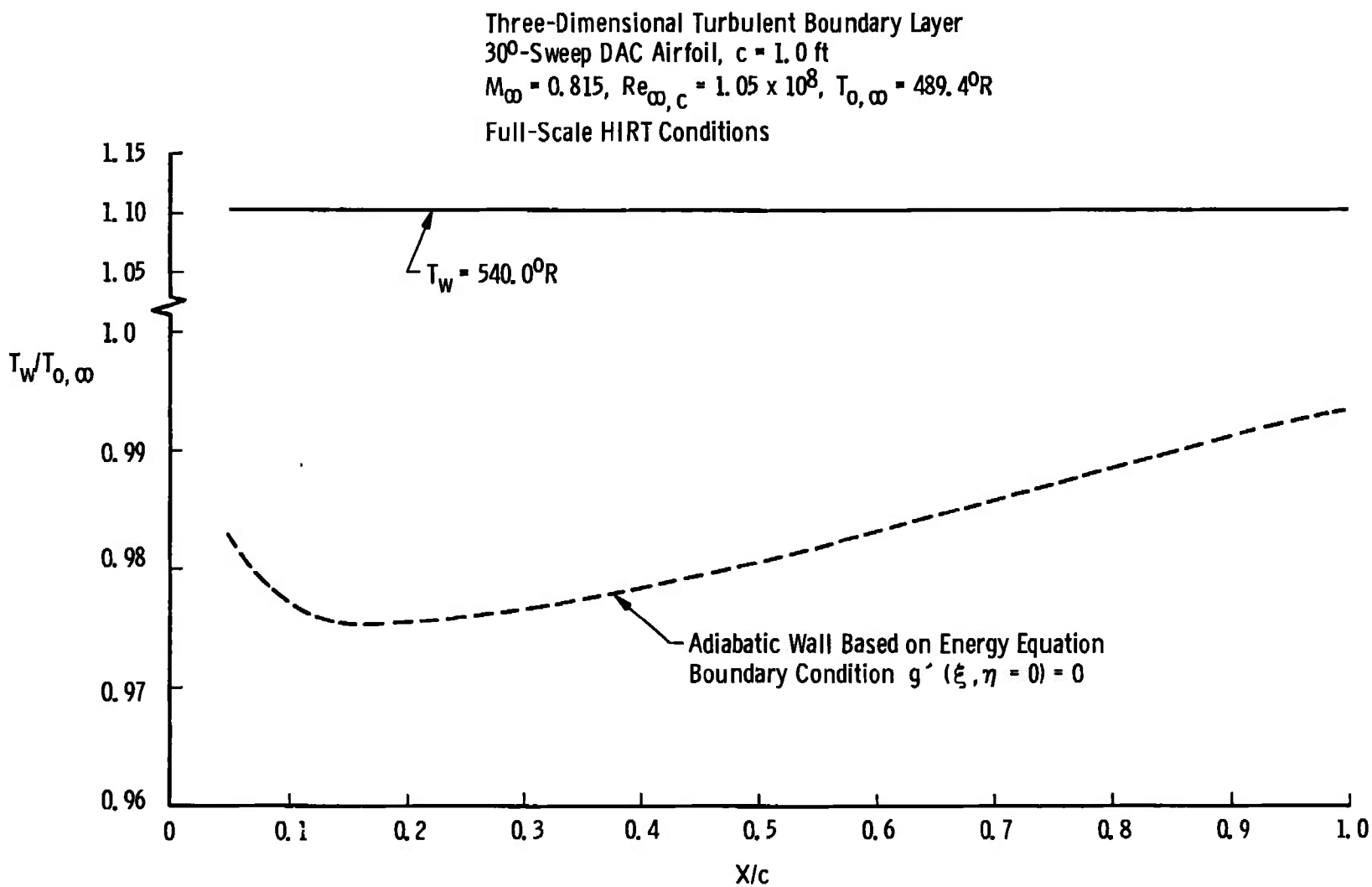

Fig. 19 Wall Temperature Distributions on the DAC Airfoil Under Full-Scale HIRT Conditions

AEDC-TR-73-156

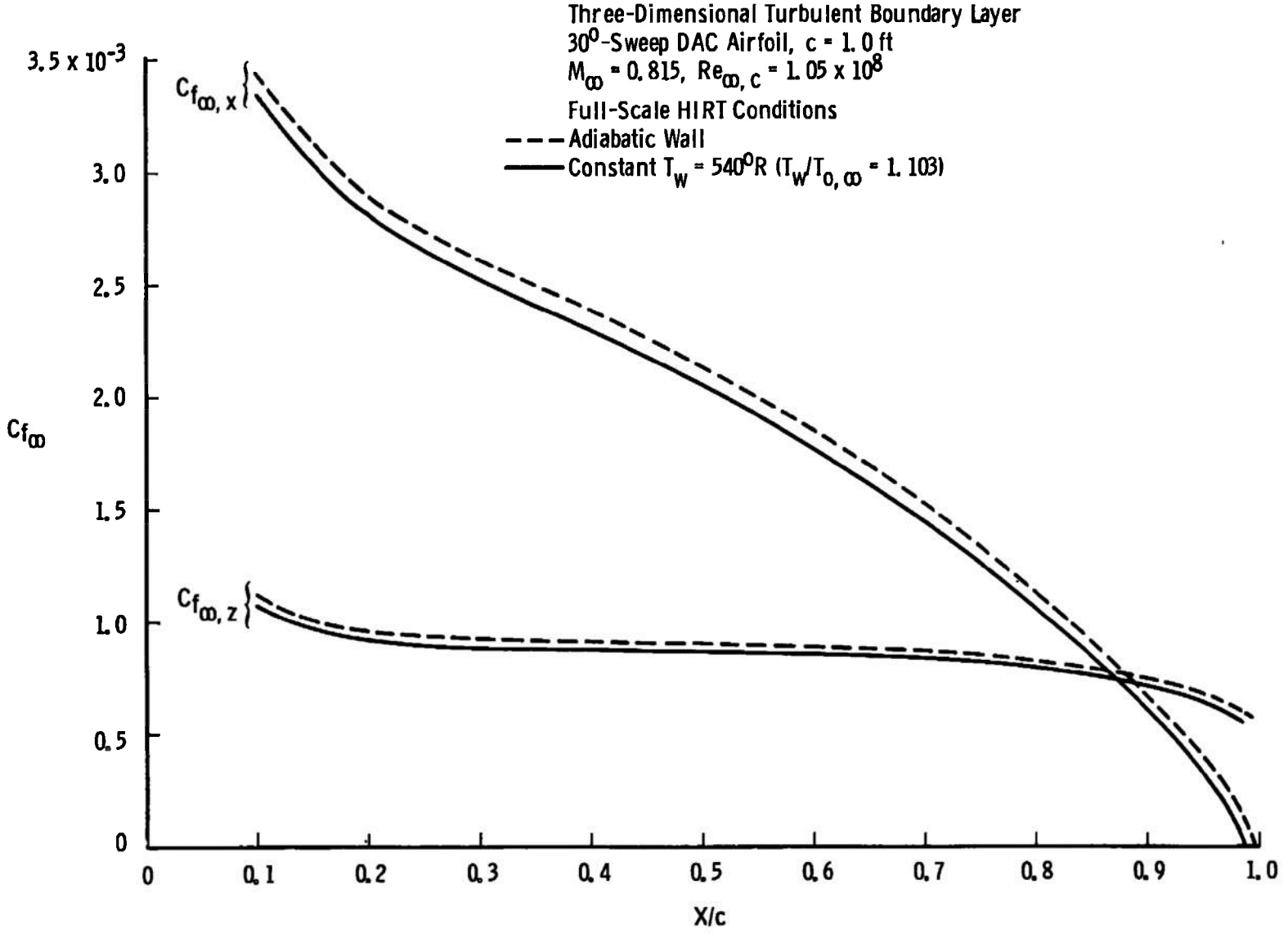

Fig. 20 Skin-Friction Coefficient Distributions on the DAC Airfoil Under Full-Scale HIRT Conditions

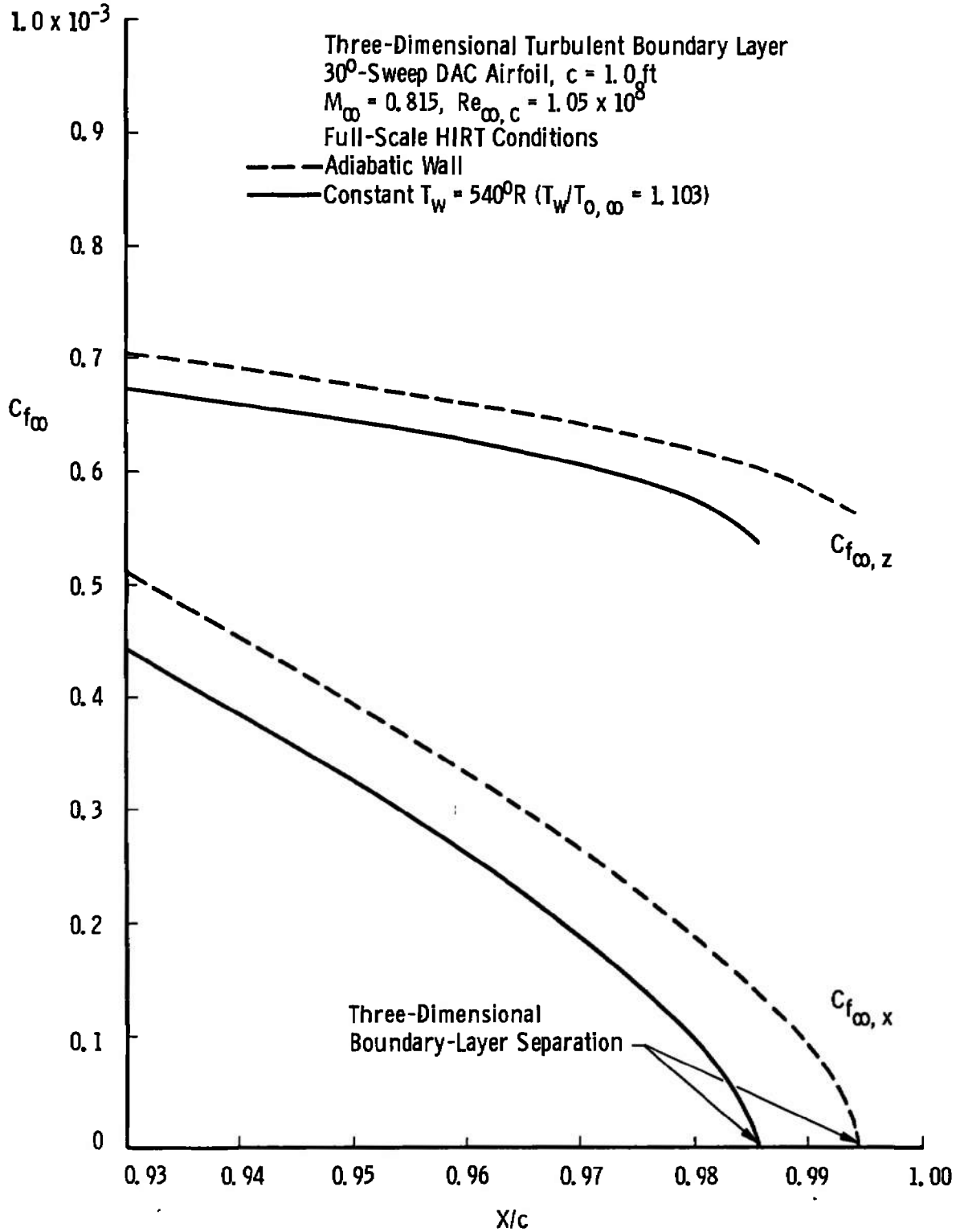

Fig. 21 Skin-Friction Coefficient Distributions Near the Trailing Edge of the DAC Airfoil Under Full-Scale HIRT Conditions

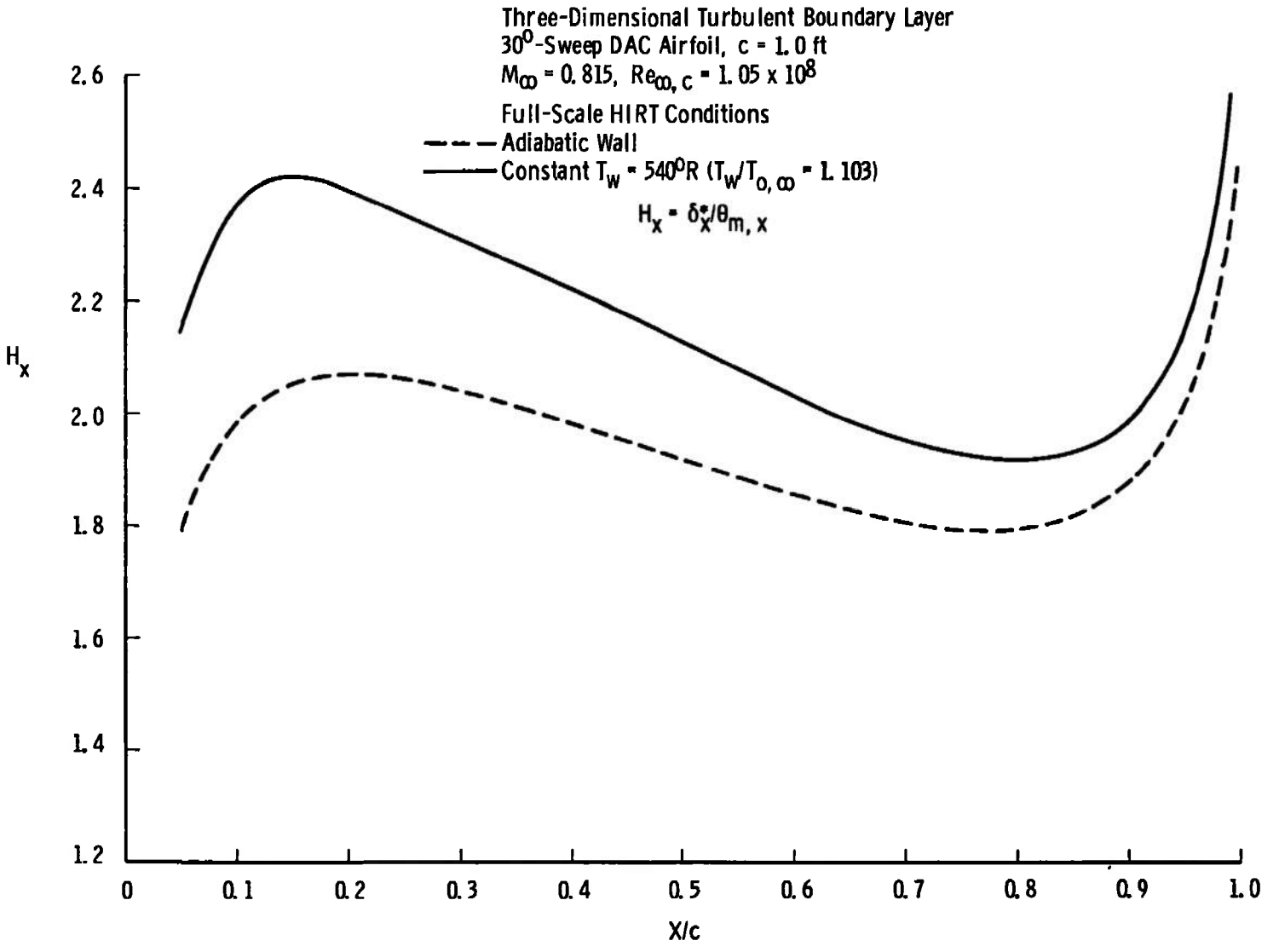

Fig. 22 x-Direction Shape Factor Distribution on the DAC Airfoil Under Full-Scale HIRT Conditions

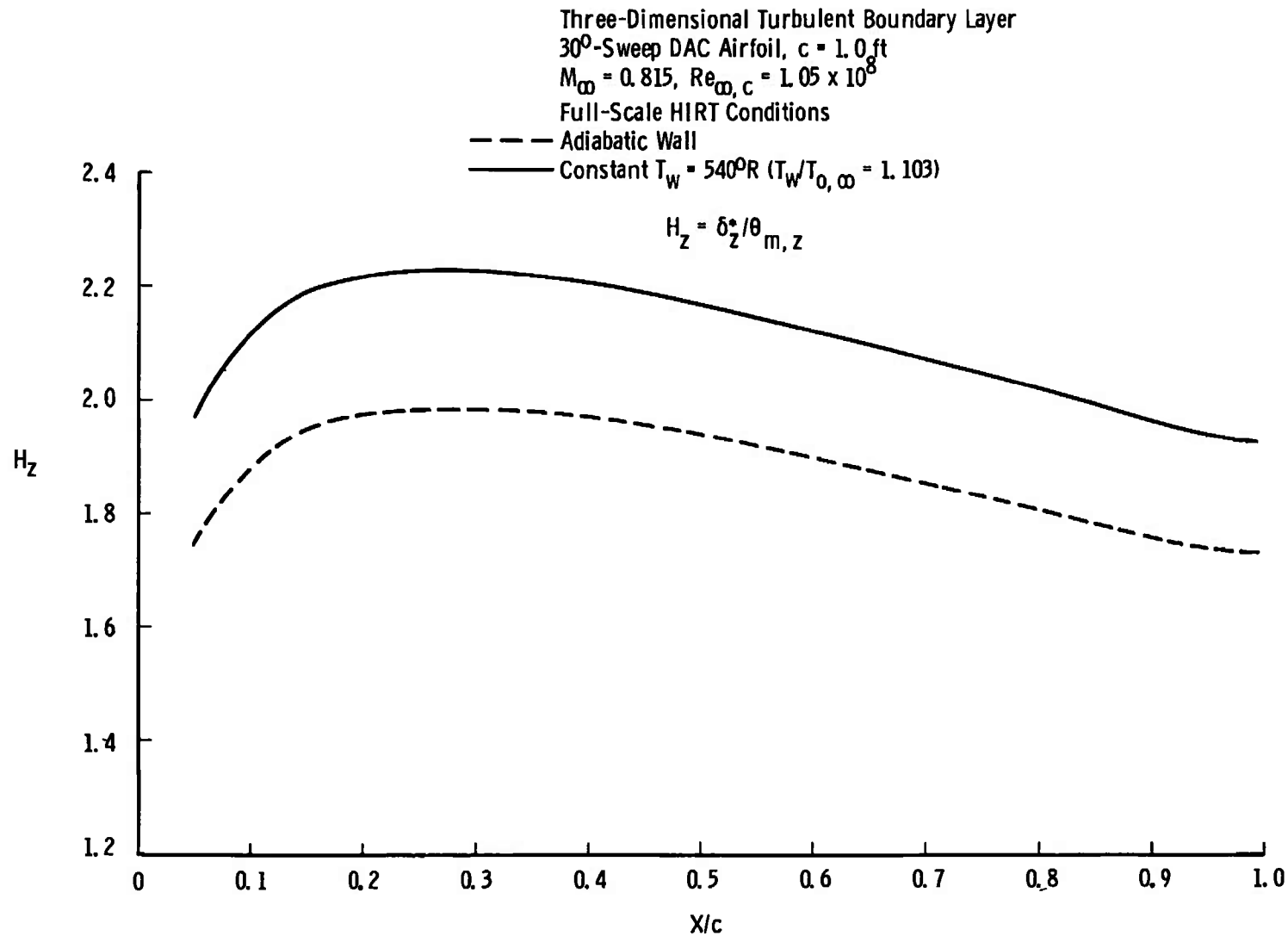

Fig. 23 z-Direction Shape Factor Distribution on the DAC Airfoil Under Full-Scale HIRT Conditions

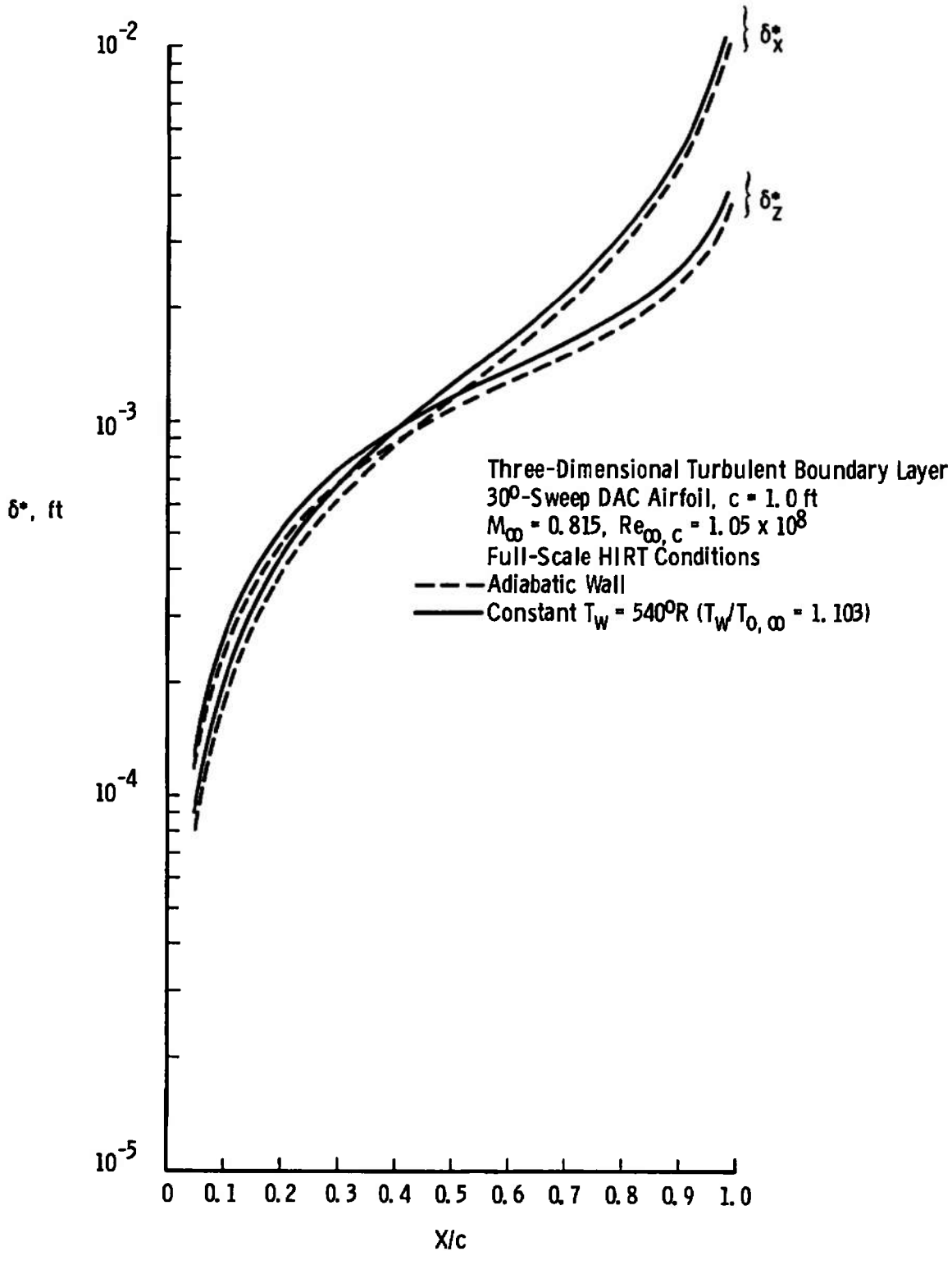

Fig. 24 Displacement Thickness Distributions on the DAC Airfoil Under Full-Scale HIRT Conditions

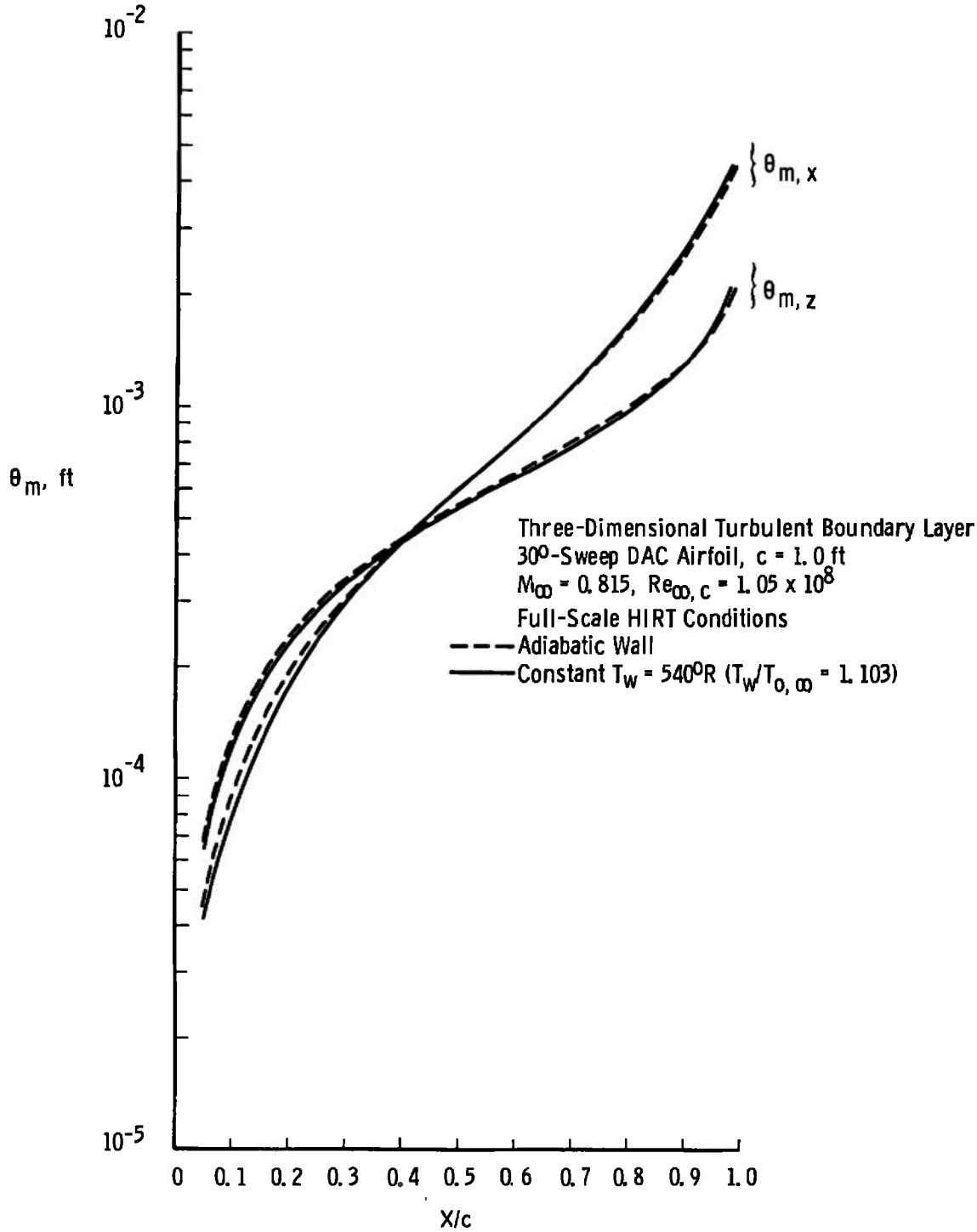

Fig. 25 Momentum Thickness Distributions on the DAC Airfoil Under Full-Scale HIRT Conditions

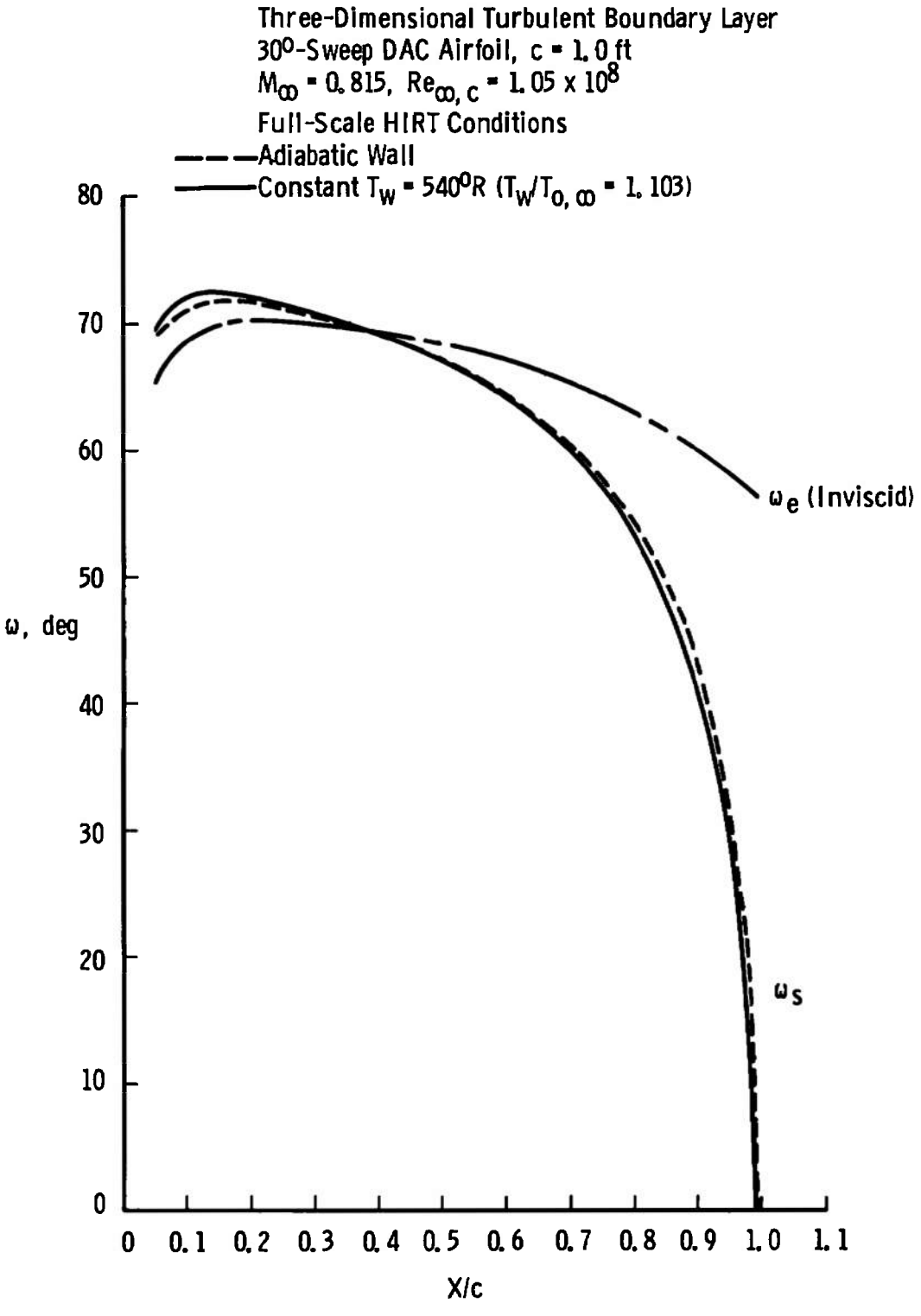

Fig. 26 Surface and External Flow Angle Distributions on the DAC Airfoil Under Full-Scale HIRT Conditions

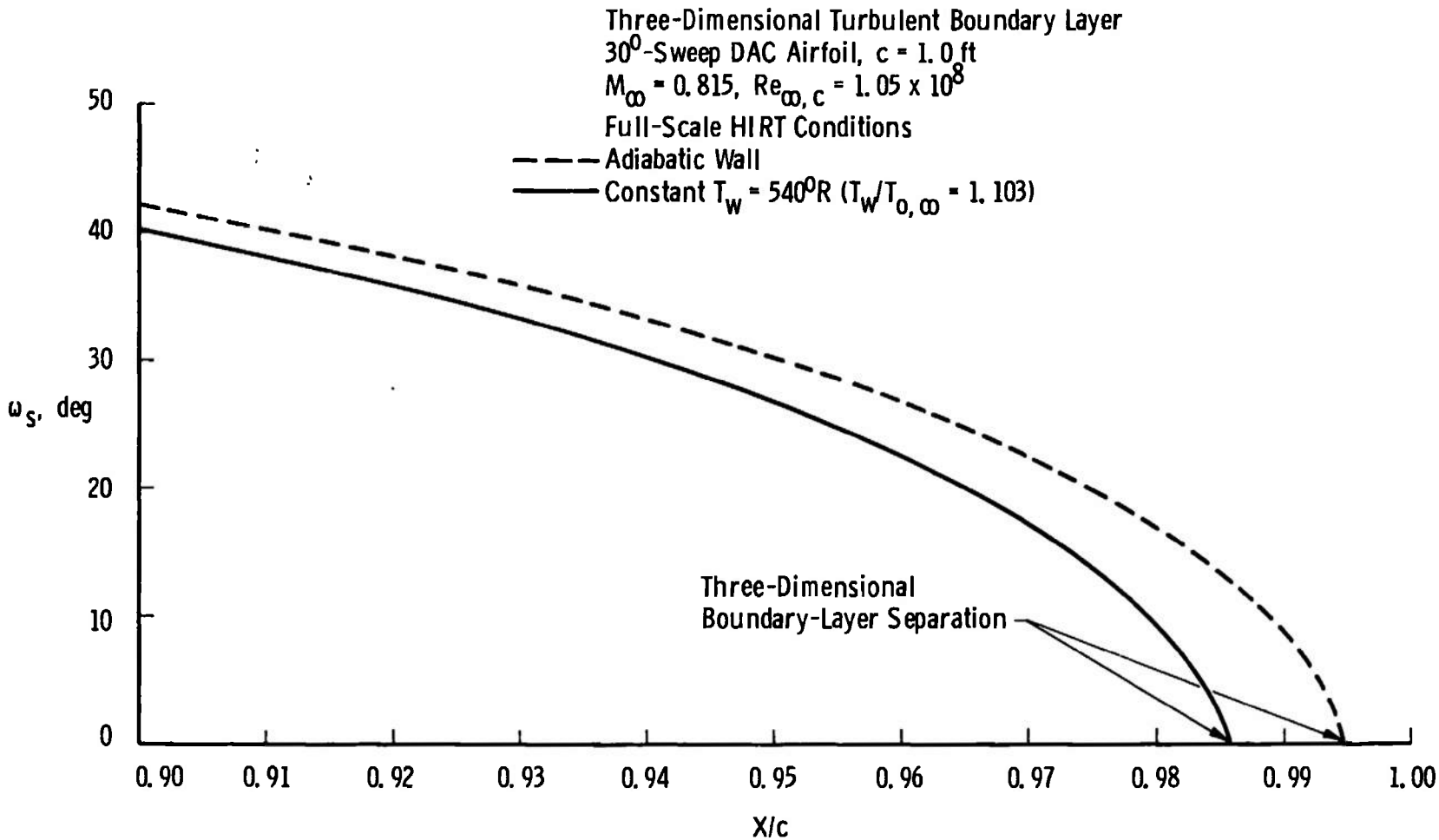

Fig. 27 Surface Flow Angle Distributions Near the Trailing Edge of the DAC Airfoil Under Full-Scale HIRT Conditions

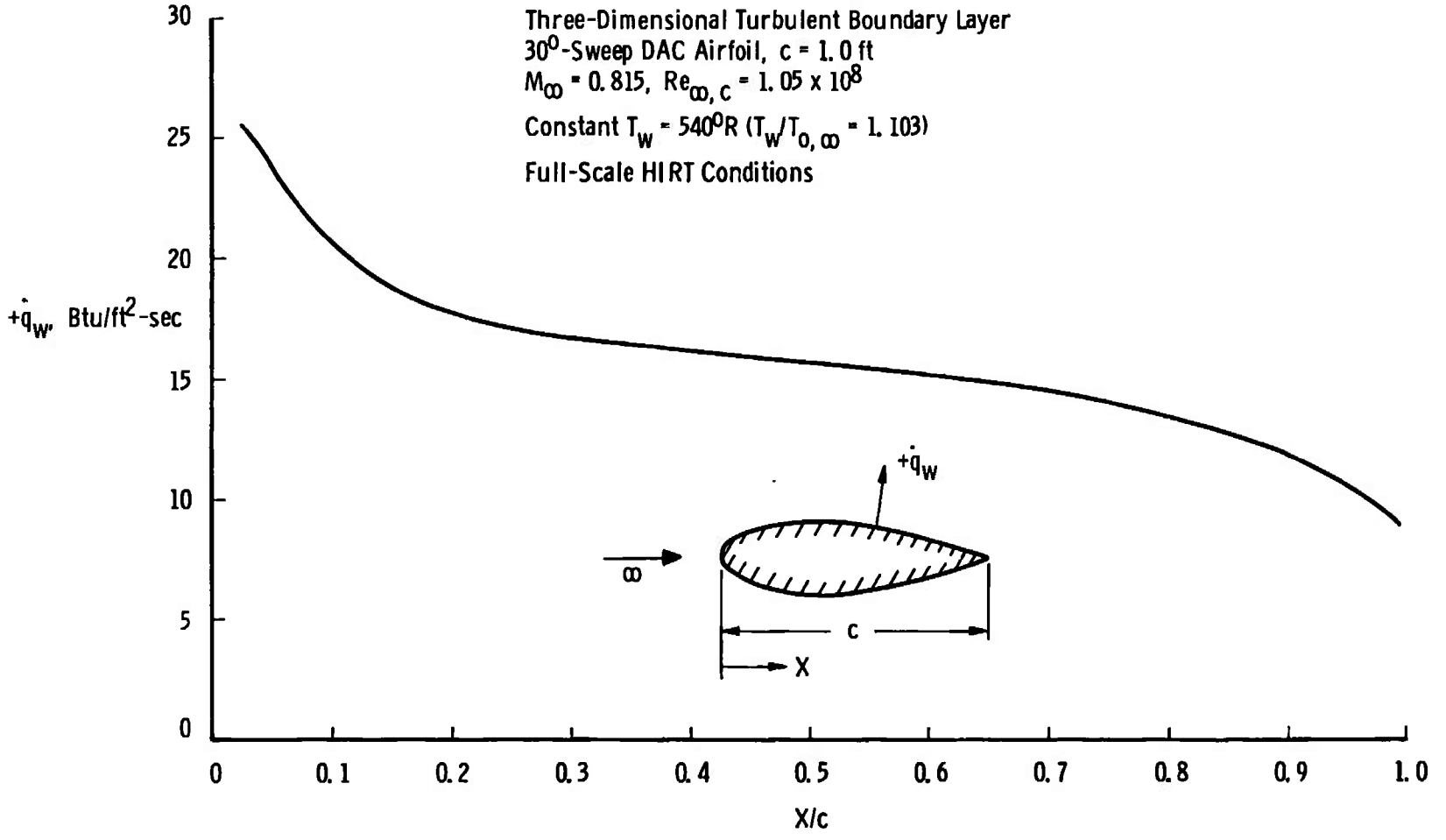

Fig. 28 Surface Heat-Transfer Distribution on the DAC Airfoil Under Full-Scale HIRT Conditions

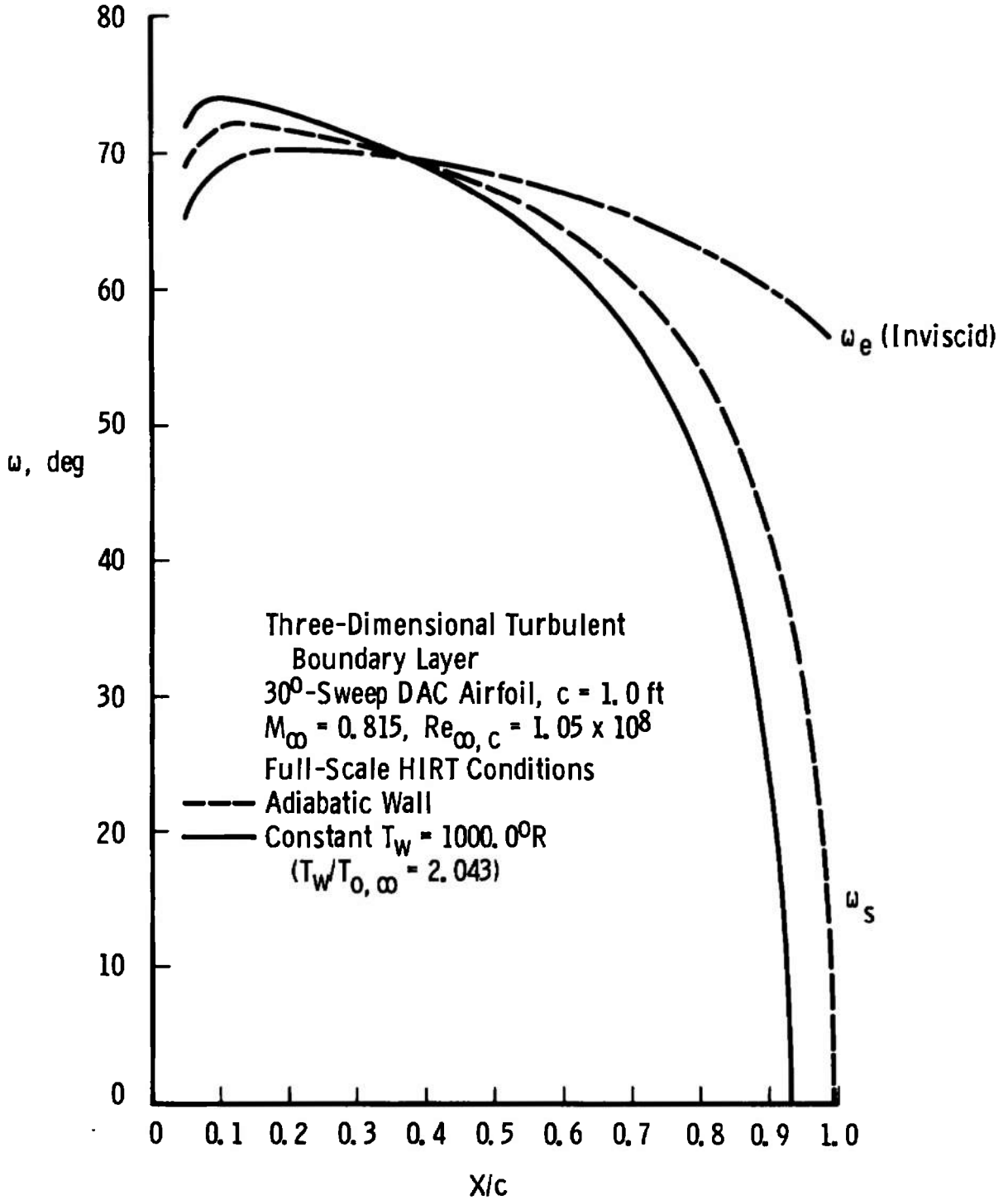

Fig. 29 Hot-Wall Effects on Surface Flow Angle Distribution

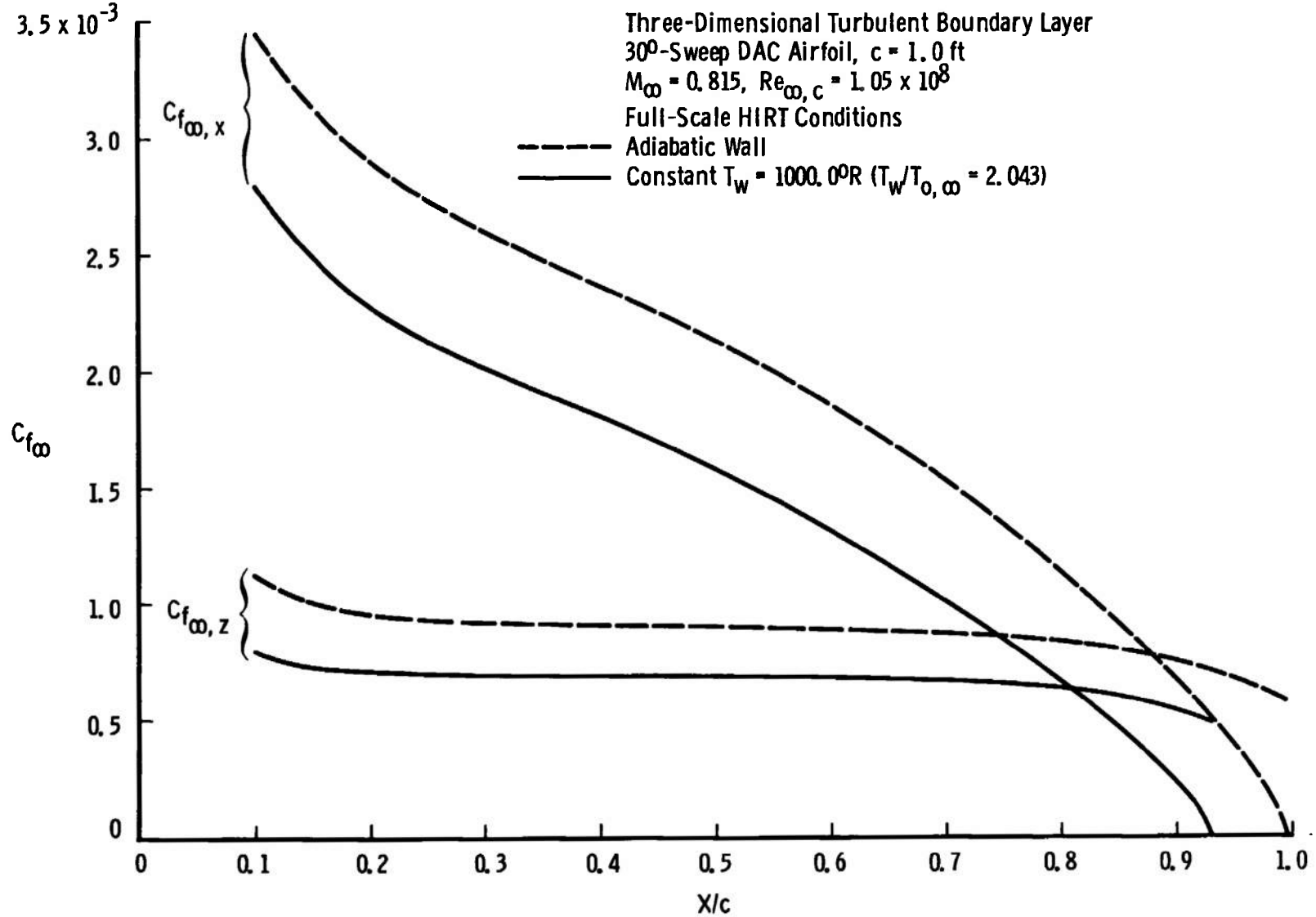

Fig. 30 Hot-Wall Effects on Skin-Friction Coefficient Distributions

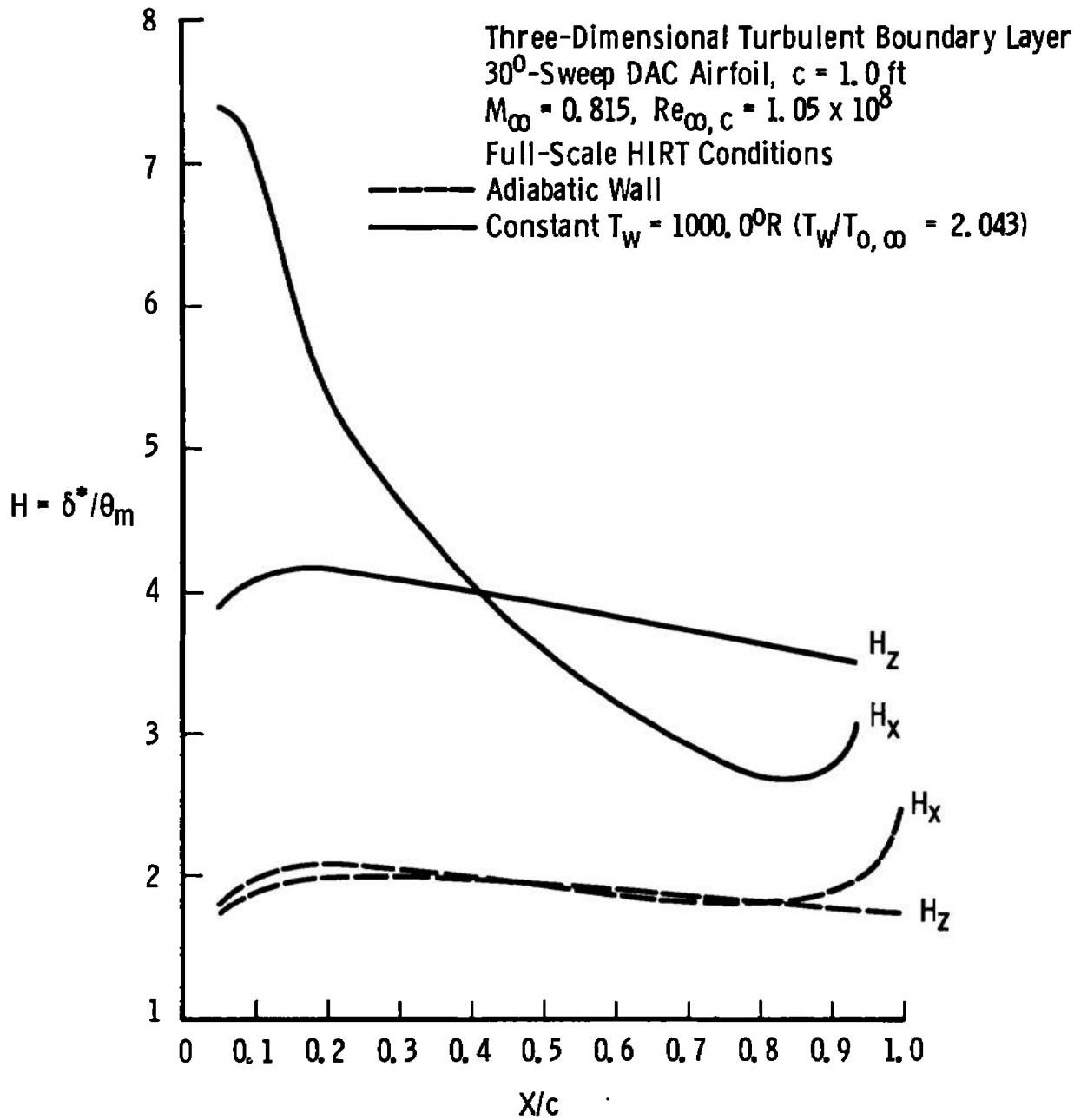

Fig. 31 Hot-Wall Effects on Shape Factor Distributions

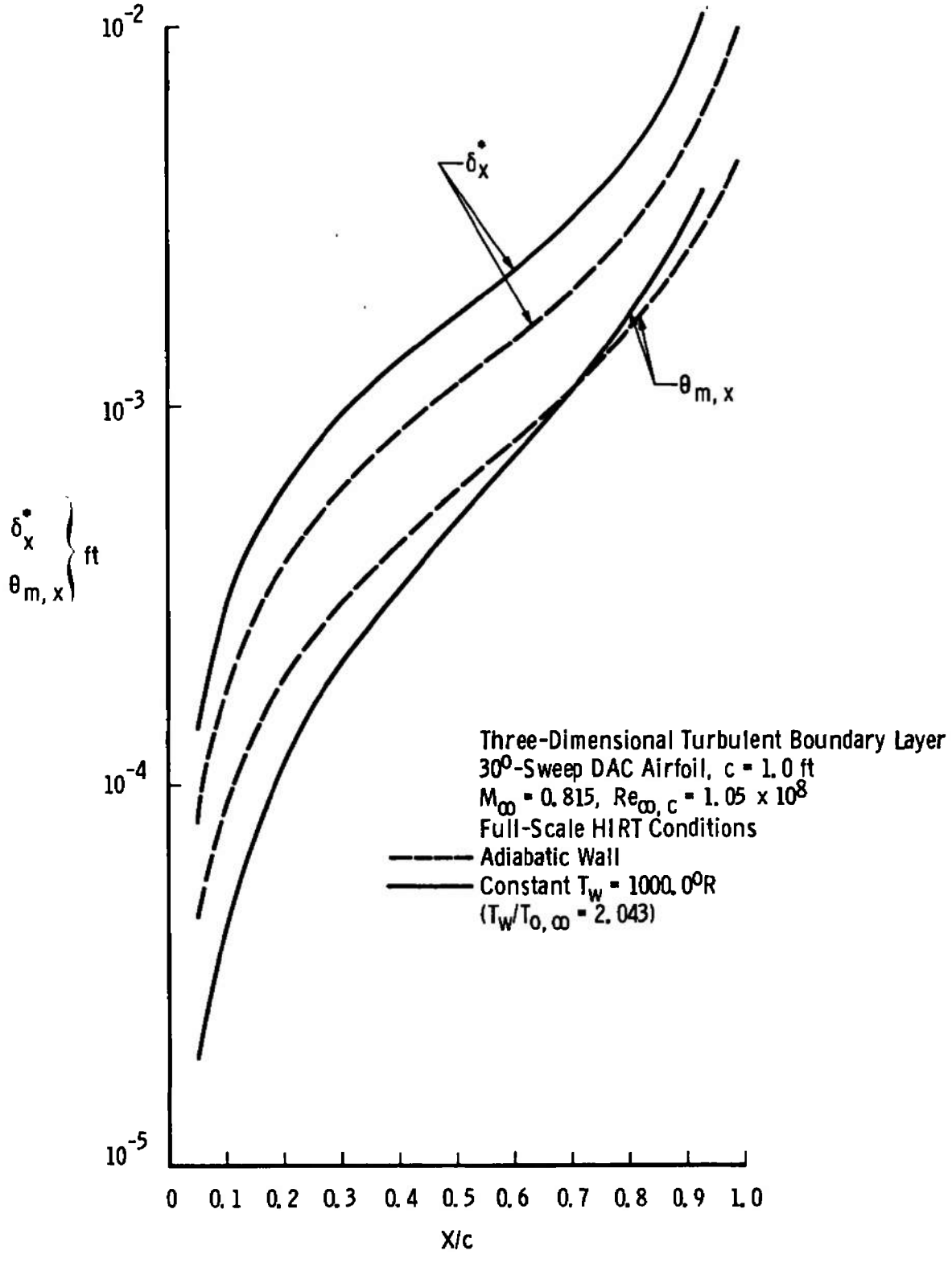

Fig. 32 Hot-Wall Effects on x-Direction Displacement and Momentum Thickness Distributions

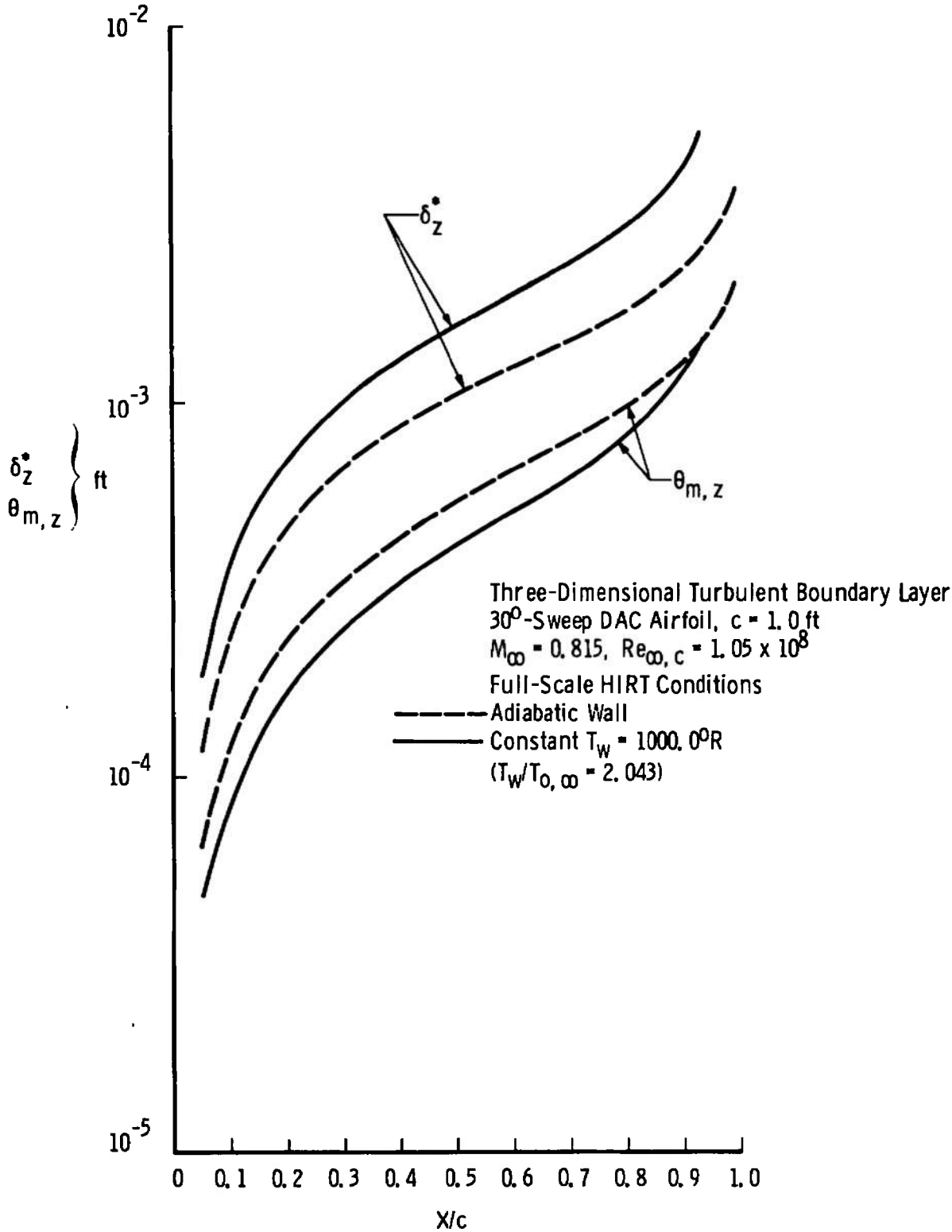

Fig. 33 Hot-Wall Effects on z-Direction Displacement and Momentum Thickness Distributions

UNCLASSIFIED

Security Classification

DOCUMENT CONTROL DATA - R & D

(Security classification of title, body of abstract and indexing annotation must be entered when the overall report is classified)

1 ORIGINATING ACTIVITY (Corporate author)	2a. REPORT SECURITY CLASSIFICATION
Arnold Engineering Development Center Arnold Air Force Station, Tennessee 37389	UNCLASSIFIED
	2b. GROUP N/A

3 REPORT TITLE

WALL TEMPERATURE EFFECTS ON TWO- AND THREE-DIMENSIONAL TRANSONIC TURBULENT BOUNDARY LAYERS

4 DESCRIPTIVE NOTES *(Type of report and inclusive dates)*

Final Report -- December 1972 through July 1973

5 AUTHOR(S) *(First name, middle initial, last name)*

J. C. Adams, Jr. and A. W. Mayne, Jr.

6 REPORT DATE	7a. TOTAL NO OF PAGES	7b. NO. OF REFS
October 1973	70	27

8a CONTRACT OR GRANT NO	9a. ORIGINATOR'S REPORT NUMBER(S)
b. PROJECT NO	AEDC-TR-73-156
c. Program Element 65802F	9b OTHER REPORT NO(S) *(Any other numbers that may be assigned this report)*
d.	ARO-VKF-TR-73-100

10 DISTRIBUTION STATEMENT

Approved for public release; distribution unlimited.

11 SUPPLEMENTARY NOTES	12 SPONSORING MILITARY ACTIVITY
Available in DDC.	Arnold Engineering Development Center, Air Force Systems Command, Arnold AF Station, TN 37389

13 ABSTRACT Wall temperature effects on the two- and three-dimensional high Reynolds number turbulent boundary layer are examined for representative AEDC High Reynolds Number Tunnel (HIRT) conditions relative to flight; also considered are hot-wall conditions relative to Space Shuttle subsonic and transonic flight during earth entry. Results obtained and presented herein show significant influences of wall-to-stagnation temperature ratio on the location of boundary-layer separation and the friction drag coefficient. The present study also indicates that the model wall temperature will be rapidly changing during a typical HIRT testing period of from 2 to 10 sec if the model is initially at ambient room temperature; such a condition may be undesirable for HIRT testing in the sweeping pitch mode since unsteady aerodynamic phenomena (e.g., airfoil dynamic stall) can be influenced by rapidly changing turbulent boundary-layer wall temperature levels. Ground testing of Space Shuttle configurations under continuous transonic flow conditions with an adiabatic wall may not be totally applicable to actual Shuttle entry, where the wing surface temperature can reach soak values on the order of twice the free-stream stagnation temperature because of the hypersonic high heating phase of the reentry trajectory. Simulation of this hot-wall/cold free-stream environment using electrically heated models appears necessary for continuous subsonic and transonic wind tunnel testing of Shuttle configurations, especially for aerodynamic drag and stall characteristics determination.

DD FORM 1 NOV 65 1473

UNCLASSIFIED

Security Classification

UNCLASSIFIED

Security Classification

14. KEY WORDS	LINK A		LINK B		LINK C	
	ROLE	WT	ROLE	WT	ROLE	WT
lifting reentry vehicles						
surface temperature						
turbulent boundary layer						
heat transfer						
Reynolds number						
aerodynamic characteristics						
aerodynamic drag						
transonic flow						

1 HIRT

2. Reentry bodies -- Boundary layer

3 " " " -

Temperature effects

AFSC
Arnold AFS Tenn

UNCLASSIFIED

Security Classification